UNIVERSITY OF CALIFORNIA
RIVERSIDE

Mathematical Model for Studying Combined Effect of Individual Cell Behavior on Developing Tissue Shape in Plants

A Dissertation submitted in partial satisfaction
of the requirements for the degree of

Doctor of Philosophy

in

Mathematics

by

Mikahl Banwarth-Kuhn

March 2019

Dissertation Committee:

Dr. Mark Alber, Chairperson
Dr. Weitao Chen
Dr. Amir Moradifam

The Dissertation of Mikahl Banwarth-Kuhn is approved:

Committee Chairperson

University of California, Riverside

Acknowledgments

I want to extend my deepest gratitude to my advisor Dr. Mark Alber for taking me on as a student during his first year at UC Riverside and investing countless time and resources into helping me grow as a student, researcher and academic. Without him I would not have found myself along my current path. I would also like to acknowledge every professor in the Math department at University of Portland during 2009-2011, especially Dr. Hannah Highlander and Dr. Chris Lee who were instrumental in convincing me I was capable of successfully completing a PhD in math and helping me apply to graduate programs. In addition, I would like to thank all the members of the applied math research group at UC Riverside, including Dr. Ali Nematbakhsh who provided invaluable support while I began my research and continued to provide extremely helpful insight throughout my time as a graduate student, Andrew Whitaker who spent his summer teaching me C++, and all the members of Dr. Venu Reddy's lab in the Department of Botany and Plant Sciences at UC Riverside. Finally, I would like to thank the humans that made my days so much brighter during my time at UC Riverside, Sam and Jolene Britton, Adam Yassine, Kevin Tsai, Josh Buli, Bryancito, Ryan and Bree Moruzzi, and Eddie Voskanian, I could not have asked for better colleagues to learn and study alongside and it has truly been an honor creating lifelong friendships with each of you.

To my wife and family, Bayley, Mom, Dad, Cletus and Brynna, for unconditional love and support every day of my life.

ABSTRACT OF THE DISSERTATION

Mathematical Model for Studying Combined Effect of Individual Cell Behavior on Developing Tissue Shape in Plants

by

Mikahl Banwarth-Kuhn

Doctor of Philosophy, Graduate Program in Mathematics
University of California, Riverside, March 2019
Dr. Mark Alber, Chairperson

The development of an organ or organism is a complex process that includes many interacting components. Scientific inquiries in developmental biology have motivated the creation of novel mathematical tools to better understand how distributions of cellular identities and phenotypes are attained through spatiotemporal regulation of cell behaviors and gene regulation. One of the central problems in animal and plant developmental biology is deciphering how chemical and mechanical signals interact within a tissue to produce organs of defined size, shape, and function. Plant development is much different from animals since the majority of organs are continually produced throughout the life of the plant and the presence of the cell wall imposes a unique constraint on cell behaviors. How exactly cell wall mechanical properties influence cell behaviors that lead to stem cell maintenance and correct organ formation is still largely unknown. To address this problem, a novel, subcellular element model of growth of stem cells within the multilayered shoot apical meristem (SAM) of Arabidopsis thaliana is developed and calibrated in this thesis using experimental data. Novel features of the model include separate, detailed descriptions of cell wall extensibility

and mechanical stiffness, deformation of the middle lamella, and increase in cytoplasmic pressure generating internal turgor pressure. The model is used to test novel hypothesized mechanisms of formation of the shape and structure of the growing, multilayered SAM based on WUS concentration of individual cells controlling cell growth rates and layer-dependent anisotropic mechanical properties of subcellular components of individual cells determining anisotropic cell expansion directions. Model simulations also provide a detailed prediction of distribution of stresses in the growing tissue which can be tested in future experiments.

Contents

List of Figures

List of Tables

Chapter 1

Introduction

1.1 Review of mathematical modeling of development

The development of an organ or organism is a complex process that includes many interacting components. Starting from an initially symmetric and almost homogeneous tissue, such as an embryo in the early stages of development, cells acquire different identities, patterns and new structures emerge, and ultimately organs form in the correct shape, size, location and orientation within the body. The highly complex nature of biological systems raises many unique challenges that have not been addressed by mathematical models in other areas of application. In particular, scientific inquiries in developmental biology have motivated the creation of novel mathematical tools to better understand how distributions of cellular identities and phenotypes are attained through spatiotemporal regulation of cell behaviors and gene regulation. During the last few decades, experiments have provided a large amount of information about the genetic composition of multicellular organisms including how genes interact, where various genes are expressed within a tissue and identification

of the primary genes involved in different developmental processes. Novel mathematical models incorporate observations from experiments to further investigate how biochemical signals interact with biophysical processes to produce the pattern and form seen in nature. Model results are then used to identify important properties of the biological system, suggest underlying general principles for development and motivate new experiments. The results of such experiments help refine models and lead to more precise predictions. In this way, modeling, combined with experiment, has become a powerful investigative tool in helping better understand complex systems in developmental biology.

1.1.1 Pattern formation and morphogenesis

Pattern formation and morphogenesis constitute a fascinating area of developmental biology with many unanswered questions. Pattern formation refers to the developmental process in which cells acquire different identities according to their spatial position within the tissue so that new organs and tissue structures develop in the correct location and orientation within the organism. This complex organization of cell fates in space and time is achieved through cell-cell signaling mechanisms that change cell identity without changing the spatial arrangement of cells. Morphogenesis is the developmental process that causes tissues and organs to develop in the shape and size necessary for proper function. This process is achieved through cell behaviors such as division, cell-cell adhesion, and cell migration that happen in response to different signals.

The first person to develop general principles for how variations in the form and structure of different organisms could emerge was D'Arcy Thompson. In his work "On Growth and Form," D'Arcy Thompson characterized morphogenesis in terms of physical

forces and mechanics [118]. Since then, many different modeling approaches have been developed to address the role of biomechanics in developmental processes. These models help to better understand the underlying physical mechanisms of important developmental processes such as tissue folding, invagination, and intercalation.

Over the past few decades, molecular level studies have revealed that a wide range of developmental phenomena are regulated by complex networks of cellular and molecular interactions [108, 114, 84, 87, 81]. The vast range of intricate pigmentation patterns and complex skeletal structures seen in both plants and animals raises the question of what type of molecular interactions are necessary to generate such elaborate patterns and form. Dynamical systems models in which cells produce and interact with diffusible signals, commonly referred to as morphogens, have served as useful models to explain self-regulated pattern formation in developmental processes.

1.1.2 Partial differential equations models

Reaction-diffusion systems

Partial differential equations (PDE) models describe concentrations of species moving through a spatial domain that is either fixed or changes throughout time. For example, PDE models have been used to describe the movement of chemical signals such as molecules, proteins and nutrients throughout a developing tissue. In particular, reaction-diffusion systems that capture the dynamics of two or more interacting chemicals have attracted a lot of interest as possible mechanisms for pattern formation in biology ever since they were formally introduced by A.M. Turing in the middle of the last century [120]. In these systems,

each chemical species has an associated diffusivity and the concentration of each chemical changes through specified biochemical reactions. These systems include both positive and negative feedbacks since there is an activator chemical that activates the production of itself and other chemicals and an inhibitor chemical that inhibits the production of the activator.

The simple mathematical model first proposed by Turing showed that a system of chemical reactions with stable, spatially uniform dynamics in the absence of diffusion could be driven unstable in the presence of diffusion and ultimately lead to spatially nonuniform patterning. Turing's ideas were later generalized and reinforced as a possible biological mechanism for pattern formation when Gierer and Meinhardt published a realistic reaction-diffusion system that undergoes this type of instability and reproduces patterns seen in experiments [42]. The equations below for a one-dimensional example describe the changes in concentrations in space and time as functions of the local concentration of the relevant substances being modeled. More specifically, the following set of equations describes the local change of the concentration of the activator chemical a and the concentration of the inhibitor chemical h per unit time [42].

$$\frac{\partial a}{\partial t} = \frac{\rho a^2}{h} - \mu a + D_a \frac{\partial^2 a}{\partial x^2} \tag{1.1}$$

$$\frac{\partial h}{\partial t} = \rho a^2 - \nu h + D_h \frac{\partial^2 h}{\partial x^2} \tag{1.2}$$

The above equations can be interpreted in the following way. Equation (1.1) states that the concentration change of the activator chemical a per unit time is proportional to a nonlinear autocatalytic production term (a^2). In this model, autocatalysis is slowed down by the action of the inhibitor chemical which is represented in the equation by the term $1/h$. The term ρ, referred to as the source density, describes the ability of cells to perform

the autocatalytic reaction. Asymmetries in the source density term can have a strong influence on the orientation of the emergent pattern. The second term in the equation $(-\mu a)$ represents the degradation of the chemical a. The number of activator molecules that disappear per unit time is proportional to the number of activator molecules present. This is similar to population models that model changes in the total population as a function of the current population. For this reason, the autocatalysis term (a^2) must be nonlinear since it must have a greater overall effect on the system than disappearance by linear decay $(-\mu a)$. The concentration change of a and h also depend on the exchange of molecules with neighboring cells. This exchange is assumed to occur by simple diffusion which are represented by the diffusion coefficients D_a and D_h. Equation (1.2) can be interpreted in a similar way.

A necessary component of this model is disparate diffusion rates. More specifically, in order for pattern formation to occur, the activator chemical must diffuse much more slowly than the inhibitor [42]. The concept of diffusion-driven instability is highly counter-intuitive because it shows that the interaction of two stabilizing components leads to instability in the system. Thus, mathematical development of reaction-diffusion systems provides an example of how mathematical theory was able to motivate the discovery of a possible mechanism for emergent behavior in biological phenomena that might have otherwise been very challenging to discover from experimentation only. In addition, this work led to an important principle of pattern formation, namely, short-range activation and long-range inhibition. Reaction-diffusion models motivated by experimental observations have been very useful in better understanding many areas of developmental biology including

pigmentation patterns of animal skin, feathers, hair follicles and tooth development and patterning of the limb skeleton. [64, 55, 69, 70, 85, 133, 49, 110, 48]. In particular, the "local autoactivation-lateral inhibition" (LALI) framework was used by our group to study vertebrate limb [135, 134] These models drastically changed the way biologists approached their study of early development.

Another model of developmental processes that has been influential over the past several decades, treats pattern formation as a downstream readout by cell genomes of spatial coordinates that are specified by graded concentrations of "positional information" (PI) molecules. The French flag model, in which a one-dimensional domain is divided into three equal parts by a diffusible signal that originates at one boundary, has served as the classic example of a morphogen-mediated spatial patterning model based on PI molecules [126, 17]. Gradient models have been extensively studied in Drosophila and [96]. Later, cell movement models were developed that postulate that cells move in response to chemical and/or mechanical cues.

Keller-Segel model for chemotaxis

Cell movement models suggest that cells move in response to chemical and mechanical cues and form aggregates, a process called chemotaxis. Chemotaxis occurs when the movement of a species is influenced by chemicals in the environment. It naturally arises in a wide variety of interesting biological settings, including cancer metastasis, angiogenesis, immune system function and egg fertilization. The Keller-Segel model was the first model to consider how cells respond to chemicals by moving up chemical gradients. In this work the authors built their model by studying aggregation of the unicellular amoeba *Dictyostelium*

discoideum (Dd). Aggregation of *Dd* is a well-known biological phenomenon in which *Dd* cells emit waves of chemoattractant (cAMP) which results in the formation of clusters in space.

This process was first modeled using two coupled differential equations [53]. The first equation describes the dynamics of the cell population density, denoted by ρ. The second equation describes the dynamics of the cAMP concentration, denoted by ϕ. The explicit form of the Keller-Segel equations is given below.

$$\frac{\partial \rho}{\partial t} = D_1 \nabla^2 \rho - \alpha \nabla (\rho \nabla_\phi) \tag{1.3}$$

$$\frac{\partial \phi}{\partial t} = D_2 \nabla^2 \phi - \lambda \phi + \beta \rho \tag{1.4}$$

These equations can be interpreted in the following way. D_1 and D_2 are the effective diffusion constants for the cells and cAMP, respectively, *alpha* is a measure of the strength of chemotaxis, λ is the rate of cAMP degradation, and β is a measure of the rate of production of cAMP by the cells. Although these equations incorporate only the most basic biology of the system, Keller and Segel showed that this mechanism could explain a large variety of patterns in bacterial populations. In addition, this system has provided many useful insights into the aggregation process, such as the existence of a cAMP concentration threshold for large-scale aggregation. A separate class of models treats cells as discrete entities.

1.1.3 Cell-based modeling approaches

Due to the complexity of coordinated cell behaviors in developmental processes PDE model approaches can be very helpful in elucidating the emergent dynamics of thou-

sands of cells when making predictions about simpler mechanisms and assuming homogeneous cell populations. PDE models provide insight at the most coarse-grained level where cell identities and heterogeneities are ignored or averaged and continuous cell densities are used to describe the system. Cell densities have also be modeled using finite element methods. However, when developing a model for the behavior of a system that is composed of thousands to possibly millions of cells, one must consider where the population is phenotypically heterogenous. Usually, cell populations are highly heterogenous and it must be decided whether or not to include more biological realism at the cellular level which comes with the computational cost of being limited to smaller numbers of cells.

Recent technological advances have made it possible to identify many of the biochemical signaling pathways that play a role in pattern formation and how they influence individual cell growth and cell differentiation events that lead to morphogenesis. Individual cell behaviors are determined by complex processes in which cells respond to extracellular cues such as interaction with their environment and other cells to make decisions. Exactly how extracellular cues are established, maintained and transduced by individual cells is unknown. Molecular and live-imaging experiments investigating development and growth of multi-cellular tissues provide very large data sets that can be used for the first time to understand how cell-level processes facilitate large-scale tissue properties. Computational modeling provides a powerful framework that is complementary to experiments and allows for the integration of biochemical and biophysical data from experiments to propose and test novel hypothesized mechanisms of morphogenesis. Unlike continuous descriptions of tissue dynamics, cell-based models can more easily account for individual cell behavior,

heterogeneity in mechanical properties of cells and cell-cell interactions. Also, cell-based models can be easily extended to incorporate new biological details at the sub-cellular and cellular levels. For example, cell shape is adaptive to local forces, the number of elements can be flexibly changed to accommodate different biological components such as actin cortex, or bulk cytoskeleton, and capturing the dynamics of heterogeneous cell populations is straightforward.

Cell-based models have been successfully used to capture passive biomechanical properties of cells during tissue development and are being extended to investigate the interplay between chemical and mechanical signals in tissue morphogenesis. These models have been extensively used for the study of the mechanical feedback hypothesis in tissue growth and development, especially for study of the regulation of growth of the Drosophila wing imaginal disc as detailed in Buchman et. al [14]. As indicated in Fletcher et al. [38], cell-based modeling frameworks currently range from vertex models that approximate the membrane of each cell by a polygon, to immersed boundary and sub-cellular element models that allow for more biologically-relevant, emerging cell shapes. Thus, models that incorporate individual behaviors such as cell-cell interactions, polarity in cell growth direction, cell division, differentiation and biochemical signaling events are necessary to quantify the impact of individual cell processes on overall tissue shape, size and function [88, 122, 28, 73, 18, 78]. For this reason, a class of cell-based modeling approaches has been developed where cells are modeled as discrete entities [For reviews see 38, 117, 123, 10].

SCE modeling approach

The sub-cellular element (SCE) modeling approach is an established cell-based framework for modeling mechanical properties of individual cells as well as their components and determining their impact on the emerging properties of growing multi-cellular tissue as well as describing cellular interactions with mediums such as the ECM and fluids [104, 122, 28, 117, 73, 106, 18, 38, 13, 80, 105, 79, 4, 128, 78, 116]. The general approach was initially developed by Newman et al. [80] for simulating the detailed dynamics of cell shapes as an emergent response to mechanical stimuli. Recent applications of the SCE modeling approach show that it is flexible enough to model additional diverse biological processes such as intercellular chemical kinetics, intercellular signaling, cell differentiation and motion of cells in fluid.

In the SCE modeling approach, membrane and cytoplasm of each cell are represented using different sets of elements/nodes and their mechanical properties are described using viscoelastic interactions between elements/nodes resulting in coarse-grained molecular dynamics type representation of the cytoskeletal network. Biomechanical and adhesive properties of cells are modeled through viscoelastic interactions between elements represented by phenomenological potential functions that simulate close-range repulsion (modeling volume exclusion of neighboring segments of cytoskeleton) and medium-range attraction between elements of the same or different cells (modeling the adhesive forces between segments of cytoskeleton)[76].

One of the important features of the SCE modeling approach is the ability to adjust parameters of potential functions describing connections between elements to calibrate

model representations of biomechanical properties of a particular type of a cell directly using experimental data. More specifically, the SCE model can be used to perform *in silico* bulk rheology experiments on a single cell in order to scale the parameters such that the passive biomechanical properties of each cell are independent of the number of elements used to represent each cell [105]. As a result, SCE simulations can capture the underlying biomechanical properties of the real biological system and remain relevant to the real biological system regardless of the number of elements chosen to represent each cell in the model.

As indicated in Fletcher et al. [38], computational experiments follow a creep-stress protocol in which a constant extensile force is applied to the end of an SCE cell whose opposite end is fixed. Before the extensile force is released, the strain is measured as the extension of the cell in the direction of the force relative to its initial linear size. *In silico* estimates of the viscoelastic properties of cells modeled using the SCE approach have been shown in many biological applications to agree very well with *in vitro* rheology measurements [105, 127]. This indicates that the simple phenomenological dynamics of the SCE modeling approach are enough to capture low to intermediate responses of cytoskeletal networks over short timescales ($\sim$ 10s) [127]. Over longer timescales ($\sim$ 100s), cells respond actively to external stresses by undergoing cytoskeletal remodeling, and this phenomenon can be incorporated into the SCE modeling approach by inserting and removing sub-cellular elements of a cell in regions under high or low stress [106].

The SCE modeling approach has been used previously by our group to model platelets in blood stream, and most recently, for studying swarming of bacteria and epithe-

lial cells in an embryo [116, 128, 4, 78]. In this work, the general SCE modeling approach is applied to develop a novel model that describes combined growth of plant cells in a multilayered structure. The ability of the SCE model to represent heterogenous mechanical properties on a sub-cellular scale is different from traditional FEM methods that model the entire meristem as one continuous material. In the FEM and other continuous models, anisotropic properties are defined by assigning different material constants along independent coordinate directions. As a result, all cells or mesh elements in a tissue have the same mechanical properties. In some continuous models, small regions of cells or subsets of mesh components are given heterogenous mechanical properties, but there is no variation on the sub-cellular scale.

The generalized Morse potential functions implemented in our model are commonly used in physics and chemistry to model inter-molecular interactions [107] and in biology to represent volume exclusion of neighboring regions of the cytoskeleton [116, 128, 4, 78, 18, 43]. It is difficult to associate specific potential functions directly with specific cytoskeletal components of cells. However, computational studies of bulk properties at the tissue level have suggested that the precise functional form of the potential used in the model has a small impact on the overall system dynamics [105, 88]. An important feature of the SCE modeling approach is the ability to adjust parameters of potential functions describing connections between elements to calibrate model representations of biomechanical properties of a particular type of a cell directly using experimental data [105]. In this work,the novel SCE model is used to perform simulations of deformation of a single cell to determine parameter values such that the passive biomechanical properties of each cell

would be independent of the number of elements used to represent each cell.

Analytical approximations from discrete models

A large body of literature exists for studying continuous limits of point-wise discrete models of biological systems. One main example includes the classic Keller-Segel PDE model of chemotaxis that was derived from a discrete model with point-wise cells undergoing a random walk. In addition, a system of macroscopic nonlinear reaction-diffusion equations was derived from the stochastic discrete cellular Potts model (CPM) along with the existence of global classical solutions to a generalization of that system. Establishing continuous limits for point-wise discrete models has many important implications for estimating qualitative behaviors of large numbers of cell such as determination of conditions promoting the formation of aggregation patterns and other self-organizing behavior.

In addition, existence of global classical solutions provide mathematical justification for using numerical solutions of discrete systems for modeling cellular behavior.

1.2 Plants Compared to Animals

1.2.1 Basic developmental similarities and differences

Growth control at the level of organs and organisms raises fundamental questions in both animal and plant biology. The last common ancestor of plants and animals is thought to be a unicellular ancestor that existed 1.6 million years ago [72]. As a result, plants and animals have evolved independent developmental strategies. Comprehensive study of of both plant and animal development not only facilitates a better understanding of general developmental mechanisms, but also demonstrates which developmental mechanisms are lineage specific and which ones are necessary for complex multicellular development. However, mathematical and computational models used to investigate developmental mechanisms have largely focused on animal systems. The differences that exist between plant and animal systems in processes such as cell-cell signaling or mechanical properties of cells create unique challenges that warrant the development of new models. Moreover, there are several very striking differences between the developmental processes in plants and animals that must be carefully considered.

A major difference between plant and animal development is that in animals, the body plan and all organ tissues are formed during embryogenesis. This means that animals are fixed in their growth pattern, i.e. all limbs and tissues are formed as a fetus and continue to grow for a period of time. In addition, after a certain age animals do not grow

or reproduce any longer. In plants, the growth and development process is much different. The plant embryo is very simple and the majority of organs are formed post-embryonically. Clusters of actively dividing cells called meristems contain pluripotent stem cells which are maintained throughout the life of the plant. The presence of a constant collection of stem cells allows for reiterative development and the formation of new structures throughout the life of the plant. Whereas in animals, the final shape of organism is determined in the womb and then grows in size, in plants there are indeterminate growth patterns since they are able to grow and produce new cells during their entire lifespan.

A consequence of extended morphogenesis, is that plant tissue structures and individual plant cells have tremendous developmental plasticity. For example, on the level of the organism, if a leaf or branch dies of natural causes, new cells will grow out to replace the lost part. In addition, whole plants can even be regenerated from some single cells. On the level of cells, growth direction of cells is highly anisotropic and can change based on different biophysical and biochemical signals in order to attain necessary tissue growth patterns and structures. Thus, a plant's pattern and form including the number of branches, height, number of fruiting bodies, etc., are greatly influenced by environmental factors such as light, temperature or predators. As a result, a wide range of morphologies can result from the same genotype. This high level of plasticity could be a robust developmental mechanism due to lack of mobility in plants.

On the cellular level, the most drastic difference is the presence of the plant cell wall. Unlike animal cells, each plant cell consists of a "membrane bag" or protoplast sitting inside the cell wall, a mechanically strong and dynamic extracellular matrix that is deposited

by the cell outside of its plasma membrane. The cell wall separating two neighboring cells can be viewed as having three separate regions [25], two primary cell wall regions immediately adjacent to the plasma membrane of each cell sitting on either side of the middle lamella (Figure 3.3) which acts like a strong glue. Plants respond to chemical and mechanical signals by reinforcing cell wall components to restrict growth in certain directions which results in anisotropic cell growth. Due to the glue like nature of the middle lamella and the mechanical strength of the rigid cell wall, cells do not move relative to one another during development and the final form and shape of a plant tissues and organs are due to coordinated patterns of cell polarization, cell growth, cell wall extension, and cell division. Thus, when and where cell division occurs in different parts of the developing tissue facilitates the formation of the entire plant body. This process takes the place of gastrulation in animals. Since the unique mechanical properties of plant cells play a large role in dictating the behavior or the entire system, two key challenges to modeling plant growth are (i) to create models that describe the development of complete tissues or organs in terms of single-cell dynamics and (ii) to integrate chemical signaling models with biophysical models to create a unified model of self-organization that leads to overall a shape and form.

1.2.2 Review of current models for plant growth and development

Multiple modeling approaches have been used to study various aspects of plant growth and development [For reviews see 2, 16, 51, 90]. The general concept of single cell growth due to cell wall yielding was first formalized by Lockhart [60]. He used rate equations for osmotic uptake of water and the irreversible expansion of the cell wall to model one dimensional (1D) elongation of a single plant cell. In his model, the cell wall is

represented as a viscoplastic material that behaves as a rigid body at low stress and flows as a viscous fluid at high stress. Experimental validation of Lockhart's theory confirmed that single cell growth and expansion in plant cells can be entirely described in terms of internal turgor pressure and the mechanical properties of the cell wall. Lockhart's model was later extended by Dumais et al. [29] to account for anisotropic cell wall properties. This model was used to describe tip growth in cells such as root hairs and pollen tubes.

More recently, several groups have developed two dimensional (2D) and three dimensional (3D) computational models for simulating growth and expansion of plant tissues [21, 22, 33, 40, 71, 75]. These models incorporate the basic physical principals of single cell growth as well as the mechanical interactions between cells. Cell-centered models represent individual cells as mass points connected to each other by 1D mechanical elements, such as springs. This approach has been used to model meristem growth in 3D [46, 52]. However, in simulations individual cells were found to slide alongside each other which is never observed in experiments. Vertex-based models provide a solution for restricted cell movement at low computational cost [40]. In this class of models, each cell is represented as a polygon with edges shared by neighboring cells. The edges represent the cell walls and are modeled by mechanical elements such as 1D or 2D springs or rods that connect cell vertices in two or three dimensions. For example, Dupuy et al. model cell walls as 1D beam elements that can be stretched or bent by external loads [32, 31, 30] . The strain rate of a beam is directly proportional to the turgor-induced stresses in the walls. This model was used to analyze the distribution of stresses and strains during the emergence of a primordium at the SAM.

Another approach used for modeling tissue growth and expansion in plants is the

finite-element method (FEM) [74, 82]. Hamant et al. [45] used FEM to model stress-strain patterns in the L1 layer of the SAM and correlate results to the behavior of cortical microtubule arrays in individual cells. In their model, the dome structure of the SAM was represented by a surface made up of 2D polygonal cells in 3D space. The cells in the deeper layers of the SAM were abstractly represented as a uniform pressure being applied to the surface from below. Boudon et al. [11] modeled the SAM as a dome structure made from polyhedrons that represent the rigidly connected 3D cells. Cell walls are represented by the faces of the polyhedrons and are composed of 2D elastic triangular elements. In their model, growth depends on the local modulation of cell wall mechanical properties and turgor pressure. Using flower development as a case study, Boudon et al. [11] showed how a limited number of gene activities controlling cell wall mechanical properties can explain the complex shape changes that accompany organ outgrowth.

1.2.3 Justification for using SCE model

In this work, we extend the SCE modeling approach to develop a novel detailed SCE model of multi-layered development of plant tissues (See [5] for details). To the best of our knowledge, the SCE method has never been used to model plant cells and tissue. Plant cells differ from animal cells because of, among other things, the presence of the cell wall, which imposes unique mechanical constraints. One of the advantages of the newly developed SCE model is that cellular and cell wall mechanical properties are calibrated directly using experimental data. In addition, there exists a large amount of heterogeneity in cell properties across different plant tissues. Thus, modeling development in plants warrants the use of a cell-based model to capture the impact of individual cell behaviors. Specif-

ically in this work, the use of the SCE modeling approach allows detailed representation of important sub-cellular properties that are hypothesized to have a large contribution to overall tissue shape and form. These properties include: 1) cell wall mechanical properties controlling anisotropic cell expansion, 2) middle lamella of the cell wall, and 3) increase in cytoplasmic pressure to generate turgor pressure.

Chapter 2

Biological Background

2.1 Overview of shoot apical meristems of plants

The shoot apical meristems (SAMs) of plants provide an ideal system for studying cell behavior in a morphogenetic and physiological context. Their essential function is to produce a constant population of stem cells that differentiate into cells for the development of all above-ground organs such as leaves, stems and branches (Figure 2.1).

2.1.1 Cell behaviors important to the determination of tissue shape

The SAM in model plant *Arabidopsis* is a multi-layered dome like structure consisting of about 500 cells that is subdivided into different layers and zones (Figure 2.1 B and C). The outermost L1 layer and the subepidermal L2 layer are single cell layers in which cells divide perpendicular to the SAM surface (anticlinal). Below the L1 and L2 layers, cells

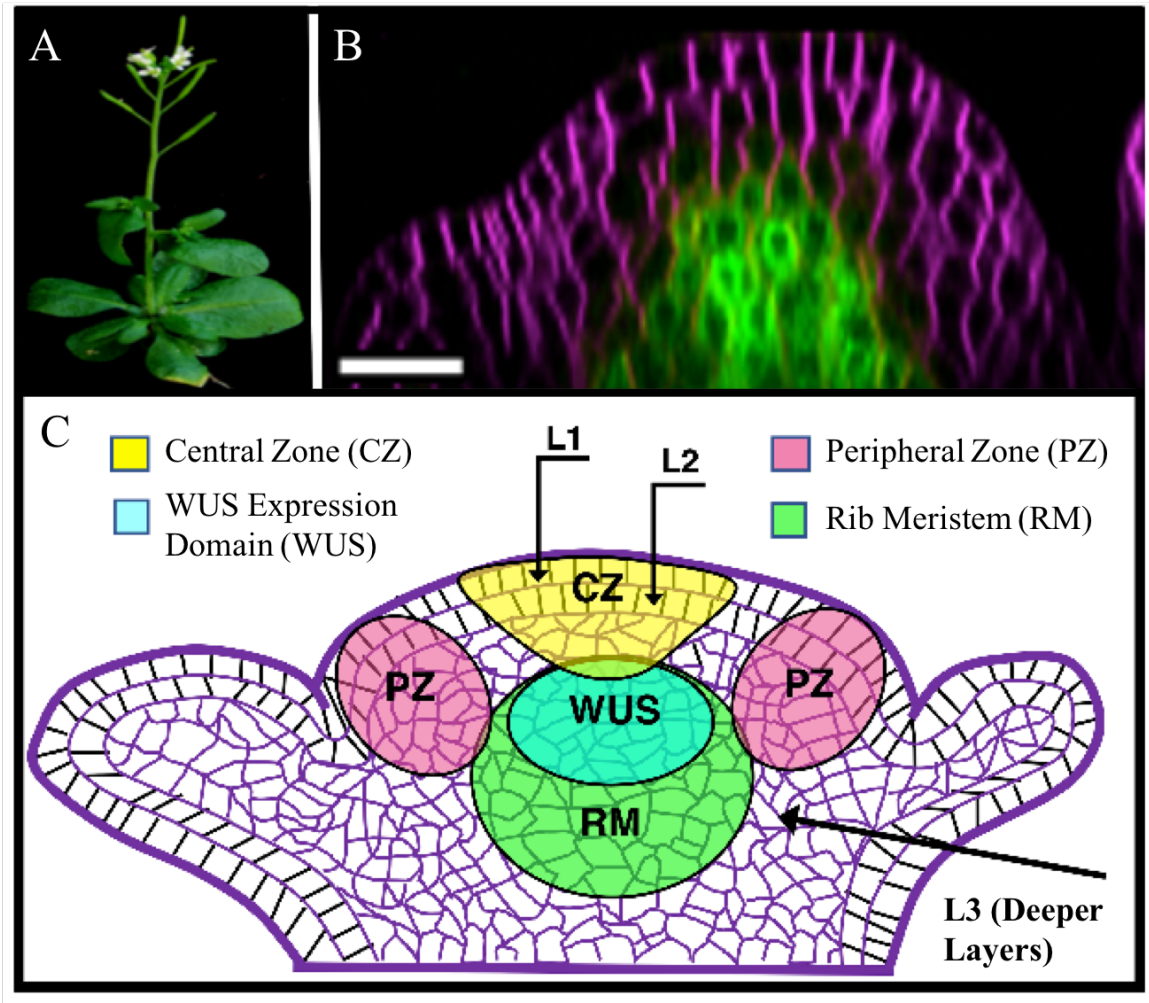

Figure 2.1: Structure and organization of the SAM. (A) The SAM is located at the growing tip of the plant. (B) Higher magnification side experimental image of the SAM showing cell layers, cell boundaries (magenta), and *WUSCHEL (WUS)* expression domain (green) in deeper layers. (C) Diagram showing different functional zones and the three distinct cell layers- L1, L2 and the deeper L3 layers. Scale bar is 25μm.

divide both perpendicular to the SAM surface and parallel to the SAM surface (periclinal) to form multiple internal layers collectively called the deeper L3 layers or corpus.

Superimposed on this layered organization, cells are also organized by functional zones. The central zone (CZ) harbors a set of stem cells that span all three cell layers (Figure 2.1 C). Stem cell progeny are pushed away laterally into the peripheral zone (PZ) where cells divide at a faster rate and differentiate at specific locations to form leaves or flowers. In addition, stem cell progeny located beneath the CZ in a region termed the rib meristem (RM), also gradually differentiate along the apical-basal axis to form the stem of the plant. Despite this process of constant displacement and subsequent differentiation, the relative ratios of cells in the CZ, the PZ, and the RM are maintained [119]. This requires a balance between two competing processes, stem cell maintenance and stem cell differentiation. Each one of these processes is regulated by a set of mechanisms controlling individual cell behaviors such as rate of growth and division, growth direction, and division plane orientation [63, 115, 129].

2.1.2 Chemical signals controlling cell behaviors

Molecular and genetic analysis has revealed critical regulators of SAM growth, stem cell maintenance, and organ differentiation [6, 92, 93, 131, 94, 52, 112, 27]. However, despite the importance of each of these factors in regulating growth and gene expression, our understanding of their feedback mechanisms is incomplete because the underlying dynamics are not well understood. Early studies show that WUSCHEL (WUS), a homeodomain transcription factor (TF) which is expressed in the RM (Figure 2.1C), is responsible for providing cues for stem cell specification in the overlying CZ [58, 67].

WUS protein migrates from the RM into the overlying CZ and specifies stem cells by repressing differentiation promoting genes (Figure 2.2) [130, 132]. In addition, WUS restricts its own transcription by directly activating a negative regulator called *CLV3* (Figure 2.2) [39, 12, 89]. *CLV3* encodes a small secreted peptide that activates membrane bound receptor kinases in order to restrict *WUS* transcription in the L1 and L2 layer and reduce *WUS* expression levels in the deeper L3 layers [19, 83]. Transient depletion of *CLV3* results in radial expansion of the *WUS* expression domain as well as a radial increase in cell division rates among stem cell daughters in the PZ [93].

Additional experiments have shown further that WUS can perform multiple functions depending upon its levels and location of expression. Misexpression of WUS in the CZ not only induces expansion of the CZ, but also results in increased cell division rates in cells of the PZ where there is low WUS accumulation [131]. Alternatively, over-activation of *CLV3* leads to a smaller CZ and an associated reduction in cell division rates. Classically, this could be correlated to a decrease in WUS levels due to down-regulation of *WUS* transcription [12, 77].

However, recent studies show that despite higher synthesis of the WUS protein in the RM of *clv3-2* null mutants, these meristems fail to accumulate higher levels of WUS in the CZ [89]. This suggests a second function for *CLV3*-mediated signaling in regulating WUS protein levels post-translationally [For details see Figure 4L in Perales et al. 89]. The presence of extremely high WUS in the inner layers and extremely low WUS in the outer layers may lead to overproliferation of epidermal cells in the outer layers along with growth restriction of centrally located cells in the deeper layers causing tissue folding and irregular

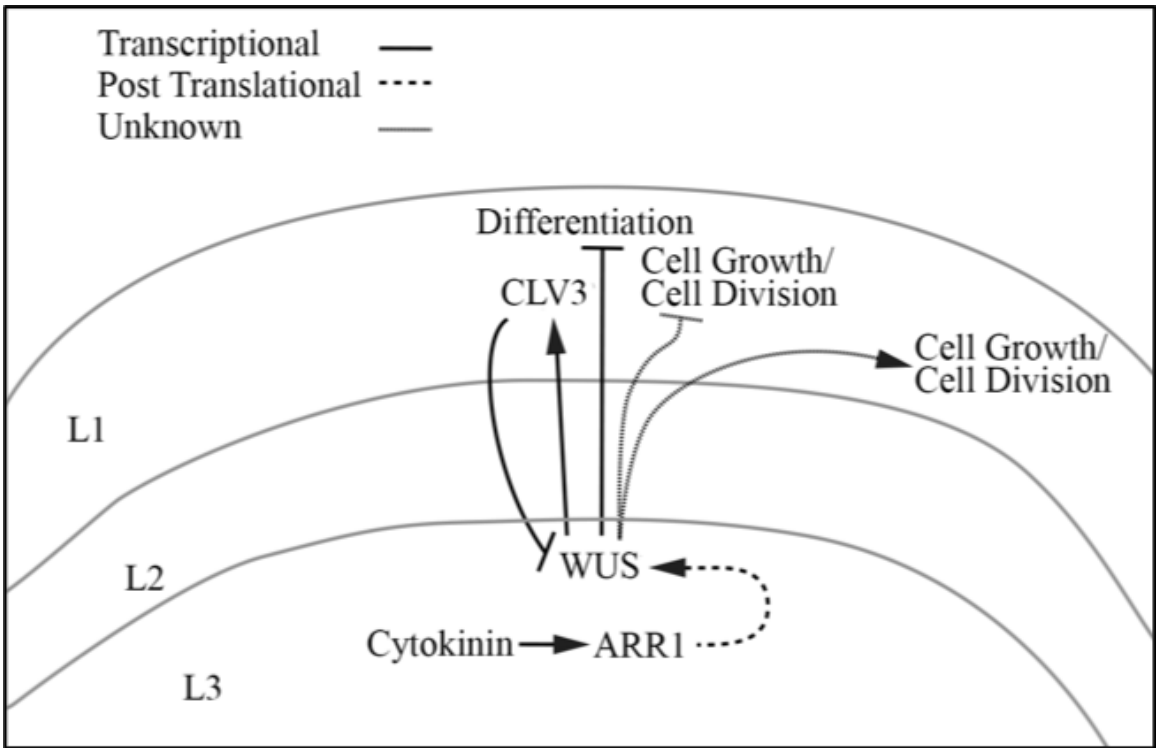

Figure 2.2: Regulatory factors in SAM growth and stem cell maintenance. Cytokinin (CK) signaling stabilizes the WUSCHEL (WUS) protein in the apical L3 layers in the RM likely through activation of TypeB ARABIDOPSIS RESPONSE REGULATOR1 (ARR1). WUS protein migrates into the CZ where it activates *CLV3* and also represses differentiation-promoting factors. In the CZ, high levels of WUS decrease cell growth and division rates either directly through an unknown mechanism or indirectly by regulating CZ identity. Similarly in the PZ, low levels of WUS are associated with an increase in cell growth and division rates.

SAMs seen in experiments. Together, these experiments suggest a more complex regulation of the WUS protein gradient, and indicate that there is no strict correlation between *WUS* transcription and WUS protein accumulation.

In addition, misexpression of WUS in the CZ results in protein instability that leads to very low, uniform accumulation of WUS and highly enlarged, dome-shaped SAMs [For details see Figure 5E in Perales et al. 89]. This suggests that lower WUS accumulation could be responsible for increased growth rates in the PZ as documented in Yadav et al. [131]. However, an increased number of slow growing cells in the central region of the SAM could either be due to expansion of the CZ identity, or to a transient, higher accumulation of WUS which was not detected in experiments because observations were made at steady-state conditions in terminal SAMs.

Recent experiments reveal that precise accumulation of WUS in space involves several interconnected, intracellular processes such as DNA dependent homodimerization, nuclear retention, and nuclear export which determine nuclear levels that impact WUS protein stability [95]. These experiments suggest that the spatial distribution of WUS impacts overall shape and size of the SAM and plays a crucial role in maintaining a constant number of stem cells. However, the exact impact of WUS levels on cell growth and division patterns in distinct functional domains and how local events influence morphogenetic processes contributing to global tissue patterns that regulate stem cell homeostasis is not well understood. This is because WUS-mediated cell fate specification, and cell growth and division patterns are spatiotemporally coupled.

2.2 Cell wall and the role of mechanical stress

In plants, the primary cell wall is composed of cellulose microfibrils cross-linked by a network of polysaccharides, including hemicelluloses and pectins [23, 25, 111, 59]. The plasma membrane of individual cells is tightly attached to the adjacent primary cell wall region through transmembrane proteins and sensors on the plasma membrane act as signals for to the cell to export new material and facilitate cell wall remodeling [59]. The plasma membrane provides a physical barrier between the cell and the primary cell wall but does not add additional mechanical strength [59]. The cell wall separating two neighboring cells can be viewed as having three separate regions [25], two primary cell wall regions immediately adjacent to the plasma membrane of each cell sitting on either side of the middle lamella (Figure 3.3). The pectin-rich middle lamella is the major physical mediator of cell-cell adhesion in plants.

2.2.1 Cell growth

One of the primary forces acting on the plant cell wall is generated by the internal turgor pressure which is strictly isotropic. However, given that plant cells often expand faster in one direction over the other [7], cell wall resistance to stress could be anisotropic. Growth anisotropy reflects the difference in the growth of a cell along one axis versus another. One way in which the degree of growth anisotropy is quantified is the difference in growth rates in the maximum direction (g_{max}) and minimum direction (g_{min}) divided by the sum of the growth rates in both directions, i.e., $(g_{max} - g_{min})/(g_{max} + g_{min})$. The meristem exhibits variability in growth anisotropy, but with an overarching pattern of increased

anisotropic growth along the axis parallel to the surface of the meristem in the L1 and L2 layers, and increased anisotropic growth along the axis perpendicular to the surface of the meristem in the L3 and deeper layers (Burian,Dumas and Kwiatkowska,Barbier).

In plants, growth direction and anisotropy are dictated by the orientation of cellulose microfibrils in the cell wall. This is largely due to the reinforcement of primary cell walls by the rigid cellulose microfibrils that have tensile strength comparable to steel [1, 7]. Cellulose microfibrils are long, filamentous structures, directly polymerized at the interface of the cell wall and plasma membrane by transmembrane cellulose synthase complexes. In cells with a preferred growth direction, adjacent cellulose microfibrils are deposited into the wall in such a way that they align parallel to one another and form bundles. As the fibrils are laid down, growth in that direction decreases [86].

The orientation and level of alignment of microfibril bundles within the cell wall is often equated to cell wall resistance since the direction of maximal expansion of the cell is perpendicular to the net orientation direction of the microfibril bundles [7]. Cortical microtubules (CMTs) guide the deposition of cellulose microfibrils (CMTs) into the cell wall [86]. Recent literature [45, 102, 103, 121, 125] provides evidence that microtubules in plant cells align along the main stress direction of the cell and therefore cellulose microfibrils are deposited into the cell wall along this same well-defined direction. Cortical microtubule response to stress relies on the dynamics of the microtubules themselves. In particular, research during the past decade has shown that the cortical microtubule network is a typical complex system, in which local interactions between individual arrays lead to emergent properties in the form of more or less aligned networks. More specifically, when they

encounter each other, and depending on the angle of the encounter, microtubules can cross each other, shrink, or zip up, and parallel alignments can emerge, as shown through particle-based simulations and probabilistic models.

Since the orientation and level of alignment of microfibril bundles within the cell wall influences cell wall resistance, plant cells have the ability to act autonomously to modify and structurally reorganize the primary cell wall to control anisotropic deformation to maintain their growth direction along the long axis of the cell and, thus, of the organ. Although the mechanism through which cortical microtubules perceive tension remains mysterious, it has been observed that compression promotes microtubule catastrophe (i.e., rapid depolymerization), but tension maintains, or even favors, polymerization (Franck, Landrein). This suggests that mechanical stress feeds back into individual cell behaviors such as anisotropic expansion direction and division plane orientation that control overall shape and size of the tissue. In addition to providing mechanical strength, the cell wall also mediates cell-cell adhesion through the pectin-rich middle lamella [25, 111, 59]. The middle lamella is primarily composed of pectin, a group of complex polysaccharide-molecules that cross-link the primary cell walls of neighboring cells. Adjacent pectin chains are cross-linked by calcium ions which facilitates cell-cell adhesion in plants [25, 111, 59].

2.2.2 Cell division

Regulation of division plane orientation of individual cells is one mechanism multicellular organisms use to control the shape of their tissues. The orientation of cell division planes has been thought to rely on cell geometry, i.e. cells usually divide along the shortest plane. This is often referred to as Errera's rule. However, in parallel to the geometric rule,

cell division planes have also been proposed to be determined by mechanical forces. Previous experimental studies have revealed a link between tension and division plane orientation in plant cells [62, 61]. Before plant cells enter mitosis, cortical microtubules reorganize into a ring called the preprophase band (PPB). This is a cytoskeletal structure that forms a closed loop around the cell. The PPB is disassembled before the cell enters mitosis, but its location predicts where the new cell plate will fuse with the previously existing cell wall [91]. There are many unanswered questions focusing on the mechanism cells use to determine the position of the PPB.

Experimental observations of pre-mitotic cells have established that cytoplasmic strands populated by microtubules and actin filaments span the space between the nucleus and the cell surface (Wick,Backhuizen,Venverloo,Flanders). Laser ablation experiments demonstrate that these strands are under tension (Goodbody, Hahne). When the cell enters mitosis, the nucleus is pulled to the middle of the cell, so it is likely that these strands are responsible for maintaining the nucleus in a central position. Such tensional forces could explain the tendency of the strands to span the shortest distance between the nucleus and the cell surface. Accumulating experimental evidence suggests that cortical microtubules align along the direction of maximal tensile stress in cell walls, implying that cortical microtubules may play an important role in cell interpretation of tension patterns in cell walls to determine cell division plane orientation [45, 121, 101]. Additionally, RM-localized CK may promote periclinal cell divisions.

2.3 Physiological implications of morphogenetic events

Understanding SAM growth and how it relates to the regulation of stem cell homeostasis, requires the study of dynamic WUS protein regulation leading to its steady-state accumulation, combined with a detailed study of how cells interpret WUS levels to specify cell identity, regulate growth patterns and determine division plane orientation. The morphological features of the SAM that arise from individual cell behaviors have important physiological implications. For example, curvature of the L1 layer of the SAM plays a role in determining the distance of the PZ from the RM, and consequently, influences how WUS accumulates in the PZ. Low WUS accumulation is necessary to allow differentiation and induction of cell division which precede primordium development. In addition, the shape of the SAM determines distribution of mechanical stress throughout the tissue which plays a role in the establishment of the main axis of expansion of individual cells and subsequently the determination of cell division plane orientation.

Therefore we developed a mathematical and computational model to study the morphological implications of individual cell behaviors in the SAM by analyzing the combined impact of WUS concentration of individual cells and mechanical properties of sub-cellular components of individual cells and the cell wall on the shape of the SAM characterized by curvature of the L1 layer. To do this, we use a novel, cell-based, sub-cellular element (SCE) model. The general sub-cellular element (SCE) modeling approach has been used before in different biological contexts. The main novelty of our model is the extension of the general SCE modeling approach to develop a novel model that enables systematic testing of new hypotheses about the underlying mechanisms driving SAM morphogenesis,

as well as application of this model for making specific, biologically-relevant predictions.

Chapter 3

Description of the Model

3.1 Novelty of multi-scale mathematical model components

In this work we have proposed using our novel computational model, a new mechanism for SAM growth which is based on WUS concentration of individual cells controlling cell growth rates and layer dependent anisotropic mechanical properties of sub-cellular components of individual cells determining anisotropic cell expansion directions across the L1, L2 and deeper L3 SAM layers (See [5] for details). The first novel model component is the detailed description of the modification and structural reorganization of the cell wall on a sub-cellular scale. In simulations, the mechanical properties of the cell wall not only vary across the different cell layers of the SAM, but mechanical properties of different sections of the cell wall vary within each individual cell. We use calibrated model simulations to quantify how layer dependent anisotropic cell wall properties representing changes in local cell wall stiffness and extensibility determine the main axis expansion of individual cells and curvature of the SAM characterized by the curvature of the L1 layer of the SAM.

The second novel model component is the detailed description of increase in cytoplasmic pressure generating internal turgor pressure. Previous computational models of the SAM growth have assumed equal turgor pressure across all cells. In our model, the internal turgor pressure of a cell is the result of interactions between internal and cell wall nodes whose displacement is affected by growth rate and anisotropic cell wall properties. As a result, turgor pressure is non-uniform across the tissue and simulations predict a detailed distribution of stresses in the growing tissue.

The third novel model component is that our model is the first model that predicts how combined growth of the three cell layers contributes to the shape of the L1 surface layer of the SAM. Other models are restricted to the L1 surface layer only. We model individual cell behavior across all three layers and assign cells heterogeneous characteristics such as anisotropic mechanical properties of the cell wall and different growth rates based on their location in the tissue. Model simulations of interactions of cells across the L1, L2 and deeper L3 layers that produce experimentally observed curvature of the L1 surface layer of the SAM provides confirmation for the initially hypothesized mechanism. Our model also contains a component for future study of the impact of division plane orientation on cell growth direction as well as on the shape and size of the SAM.

Previous models assume a geometric division rule, i.e. cells divide along the shortest plane [109, 98, 44, 9, 56, 99, 35]. However, a geometric division rule is oversimplified and is not related to any biologically relevant mechanism cells might use to determine their plane of division. In addition, there is experimental evidence that cells do not always follow this rule, especially when large amounts of plant hormones are present. Thus, understand-

ing how cells respond to chemical signals could lead to insight about what mechanisms govern cell behaviors. It is unclear at this time which role plant hormones and other chemical signals play in determining division plane orientation, as well as which role mechanical properties of the cell wall play. We propose to test a new SAM growth mechanism based on coordination of cell division.

Cell division is highly regulated in the meristem to arrive at the correct tissue shape both spatially, i.e. in which layer do anticlinal versus periclinal divisions occur, and temporally, i.e. heterogenous division rates amongst cells in different functional zones. Our model tests how the transcription factor WUS and the plant hormone cytokinin compete to determine division plane orientation of cells. Specifically, we test the hypothesis that WUS stops periclinal division whereas cytokinin induces periclinal division. In addition, we provide a detailed representation of the mechanical properties of the cell and the cell wall during growth and division. This includes division plane orientation based on distribution of stress on the cell wall, measuring variation of internal pressure of individual cells caused by changes in mechanical properties of the new cell wall after division and relating this variation of internal pressure to distribution of stress in the tissue, and testing the hypothesis that WUS and CK affect mechanical properties of the cell wall, i.e. WUS makes cells expand in horizontal direction and cytokinin makes cells expand in the horizontal direction, that determine growth direction of individual cells and consequently influence stress on the cell wall that leads to the choice of division plane orientation.

Lastly, our model is the first attempt to test how WUS concentration across different layers of the SAM could affect individual cell behavior leading to orderly layer formation and experimentally observed shape of the L1 surface layer of the SAM. We hypothesized that WUS concentration of individual cells controlling cell growth rate along with layer dependent anisotropic mechanical properties of subcellular components of cells reproduces cell expansion directions and shape of the L1 layer of the SAM seen in experiments. In addition, model simulations validate hypothesized mechanism based on WUS concentration of individual cells controlling cell growth rates in the deeper L3 layers, i.e. high WUS accumulation being associated with slow growth and low WUS accumulation being associated with faster growth, resulting in the experimentally observed shape of L1 layerF.

3.2 SCE computational model for stem cell maintenance and growth of the SAM

Our model simulates a 2D longitudinal cross-section of the SAM (Figure 3.1). In Reddy et al. [92] application of the live imaging techniques led to the development of a spatial map of cell growth and division patterns. Cell division rates were found to vary across the SAM surface and it was shown that cell cycle lengths are radially symmetric, i.e. cells in the PZ divide at a faster rate than cells in the CZ (Figure 3.1 G-J). In addition, the WUS signaling domain has been shown to be radially symmetric (Figure 3.1 A-C). It is important to note that symmetry in growth rates and chemical signaling domains are broken upon formation of organ primordia, but this happens outside of the domain our model encompasses (Figure 3.1 D).

Experimentally observed symmetry in distribution of growth rates and the WUS signaling domain across SAM layers supports application of a 2D model since it suggests that the apical half of the meristematic dome is radially symmetric, i.e. a longitudinal cut at any angle through the center of the meristem will give the same profile, with respect to both cell growth patterns and the WUS signaling domain within our domain of simulation. In addition, a 2D model is sufficient to predict shape, quantified by curvature of the L1 layer, since the dome-like structure of the apical half of the meristem ensures curvature of the L1 layer in longitudinal cross-sections of the SAM will be invariant under the choice of angle of the cut within our simulation domain (Figure 3.1 E-F).

In what follows, the different types of sub-cellular nodes that are used to simulate different components of each cell and the cell wall are described as well as the potential functions used to represent interactions between them. Then the approach implemented to model cell growth, cell wall elongation and cell division are described as well as the approach implemented for determining anisotropic mechanical properties of the cell wall. Finally, the equations of motion for each sub-cellular element are provided along with the numerical method used to solve them to provide a complete model description.

3.2.1 Turgor Pressure

In our model, two groups of nodes are used to represent the cell wall and internal cell domains separately (Figure 3.2). Collective interactions between pairs of internal nodes (E^{II}) represent the cytoplasmic pressure of the cell, and collective interactions between pairs of internal nodes and primary cell wall nodes (E^{IW}) represent turgor pressure, the

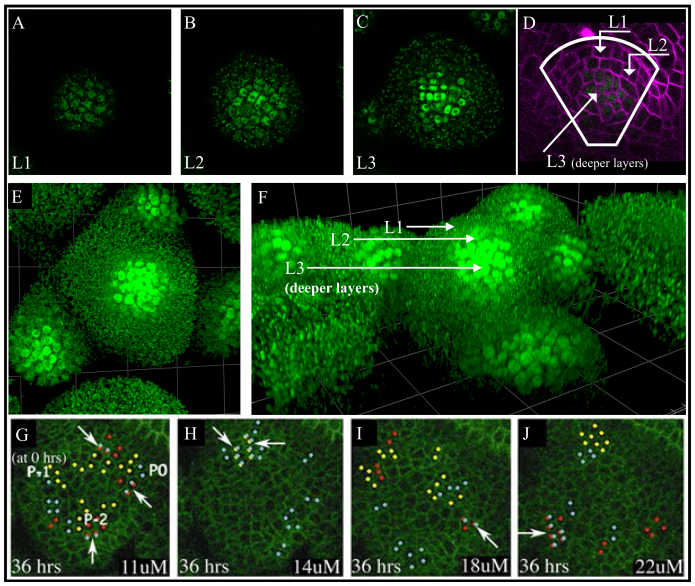

Figure 3.1: Experimental images demonstrating symmetry in distribution of growth rates and the chemical signal WUS in SAM layers as well as dome-like structure of the apical half of the meristem. (A-C) Images show individual top-down sections showing WUS protein accumulation in the L1 (A), L2 (B), and L3 (C) layers (green). (D) Experimental side-view image showing simulation domain in white. (E-F) 3D reconstructed image of the SAM displaying dome shape of the meristem as well as radial symmetry of WUS signal across L1, L2 and deeper L3 layers (green). (G-J) Spatial distribution of mitotic activity over time. Images show individual top-down sections from the same plant, depicting cells located in the L2 and deeper L3 layers at the same time point. Cells that have divided in each of the 12-hour intervals are color-coded. Red dots represent cells that divided in the first 12-hour window, yellow dots the following 12 hours, and blue dots the final 12 hours. There is low to no division in the CZ and rates increase as you move toward the PZ. The overlapping dots indicate a second round of cell division (arrows) which are only present in outermost edge of meristem. Image reprinted with permission from Reddy et al. [92].

Elements of the SCE model	**Type of potential acting on each element**	**Biological feature**
Internal-internal node (E^{II})	Morse potential	Internal pressure
Internal-cell wall node (E^{IW})	Morse potential	Turgor pressure, the force per unit surface applied on the primary cell wall by the protoplast
Cell wall-cell wall node in the same cell wall region (E^{WWS})	Linear and rotational spring potential functions	Mechanical stiffness and extensibility of the primary cell wall
Cell wall-cell wall node of neighboring cells (E^{WWD})	Morse potential	Volume exclusion of the cells due to cell wall material such as cellulose microfibrils and pectin that sit between neighboring cells and keep adjacent cell membranes from making contact
Cell wall-cell wall nodes of neighboring cells (E^{Adh})	Linear spring potential function	Middle lamella

Table 3.1: Potential energy functions in the model

force per unit surface applied on the cell wall by the protoplast (Figure 3.2 A).

Plant cells are under high internal turgor pressure, generally in the range of $0.1-1$ MPa [41], and are prevented from bursting by the presence of the cell wall. Turgor pressure is generated when water crosses the cell membrane by osmosis, and causes the protoplast (cell excluding the cell wall) to swell. Swelling of the protoplast is restricted by the cell wall and this generates turgor pressure. These interactions between pairs of internal nodes, and pairs of internal and primary cell wall nodes are modeled using Morse potential functions.

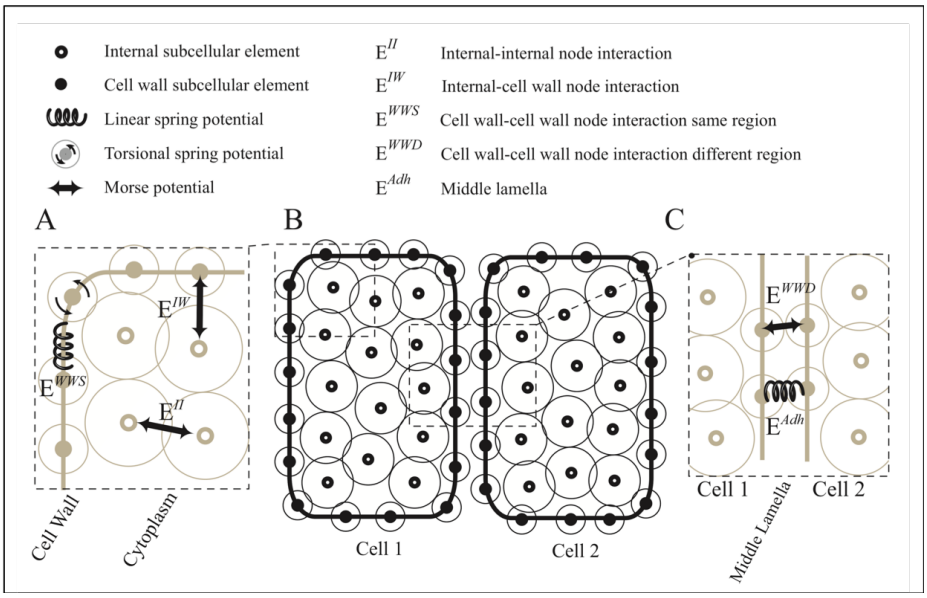

Figure 3.2: Diagram of interactions of the SCE model components represented by different types of nodes. (A) Intracellular interactions between cytoplasm and primary cell wall nodes. (B) SCE model components of two neighboring cells. (C) Diagram of the intercellular interactions between two neighboring cells involving middle lamella. Symbols and notations are described in the figure itself.

The Morse potential used in the model consists of two terms generating short-range repulsive and long-range attractive forces. The following equation is a Morse potential which models the interaction between internal node i and cell wall node j:

$$E_{ij}^{IW} = \left[U^{IW} \exp\left(-\frac{|x_i - x_j|}{\xi^{IW}} \right) - W^{IW} \exp\left(-\frac{|x_i - x_j|}{\gamma^{IW}} \right) \right] \tag{3.1}$$

where U^{IW}, W^{IW}, ξ^{IW}, and γ^{IW} are Morse parameters. The same form of the potential with different sets of parameters is used for E^{II} and E^{WWD} (Table 3.1 and Table 3.2).

3.2.2 Cell Wall and Middle Lamella

As described in (2), the primary cell wall in plants cells is composed of cellulose microfibrils cross-linked by a network of polysaccharides, including hemicelluloses and pectins [23, 25, 111, 59]. The plasma membrane of individual cells is tightly attached to the adjacent primary cell wall region through transmembrane proteins and sensors on the plasma membrane act as signals for to the cell to export new material and facilitate cell wall remodeling [59]. The plasma membrane provides a physical barrier between the cell and the primary cell wall but does not add additional mechanical strength [59]. As such, primary cell wall nodes in our model represent mechanical properties of the primary cell wall and plasma membrane together (Figure 3.2).

In our model, each region of the primary cell wall is represented with an individual set of nodes surrounding each cell. Interactions between primary cell wall nodes of the same cell (E^{WWS}) are used to model cell wall mechanical stiffness and extensibility (Figure 3.2 and Table 3.1). There are two types of interactions between primary cell wall nodes of neighboring cells (Figure 3.2C and Figure 3.3). (E^{WWD}) is a repulsive force that is modeled

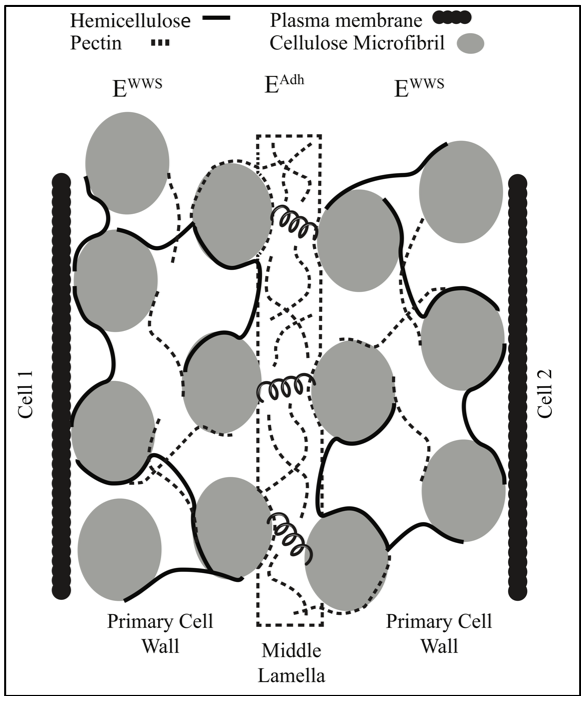

Figure 3.3: Diagram of three cell wall regions between two neighboring cells: two primary cell wall regions on either side of the middle lamella.

using a Morse potential function to prevent membranes of adjacent cells from overlapping. This represents cell wall material present between neighboring cells which keeps adjacent cells membranes from making contact. Pairwise linear spring interactions are used to model cell-cell adhesion mediated through the middle lamella (Figure 3.2 C, 3.3 and Table 3.1).

Several modeling studies have investigated the importance of microtubule dynamics in cell growth [15, 3]. Since CMTs do not contribute directly to cell wall resistance to stress [60], we developed a coarse-grained model that represents cellulose microfibrils and CMT dynamics through motion of nodes connected by linear and rotational springs. Namely, interactions that lead to anisotropic expansion through modification and

structural reorganization of the primary cell wall are represented by linear and rotational springs (E^{WWS}) (Figure 3.2A). Linear-spring interactions given by the following equation $E_{linear} = \frac{1}{2}k_{linear}(x - x_{eq})^2$ are defined between adjacent nodes of the cell wall to maintain the length of cell wall segments and regulate cell wall extensibility (See section 3.2.3). Rotational spring interactions defined between three successive nodes of the cell wall are described by the following equation, $E_{bend} = \frac{1}{2}k_{bend}(\theta - \theta_{eq})^2$ and are used to maintain a prescribed degree of bending between cell wall segments [8]. The degree of bending between cell wall segments represents the level of alignment and coordinated orientation of the cellulose microfibrils, and parameters of the bending equation were chosen to mimic cell shape observed in experimental images. Bending stiffness in the model limits cell expansion along the axis perpendicular to the preferred growth direction, similar to how cells lay down microfibrils to limit expansion in the experimental observations. The parameters k_{bend} and k_{linear} were calibrated using elastic modulus of cells measured in experiments (See section 3.2.8). In simulations, spring constants of primary cell wall nodes are varied based on cell layer and prescribed growth direction of cells leading to anisotropic mechanical properties of the cell wall.

In addition to providing mechanical strength, the cell wall also mediates cell-cell adhesion through the pectin-rich middle lamella [25, 111, 59]. In our model, pairwise interactions between cell wall nodes of adjacent cells (E^{Adh}) function as a coarse-grained model for cross-linking of pectin molecules in the middle lamella (Figure 3.2C, 3.3 and Table 3.1).

3.2.3 Cell Growth and Anisotropic Cell Wall Expansion

Live imaging techniques were previously used to analyze cell cycle lengths in real-time and generate a spatial and temporal map of cell growth and division patterns in the SAMs of *Arabidopsis* [92]. In the current model, cell growth is represented by the addition of new internal nodes at a constant rate (Figure 3.5 and section 3.2.8). When a new internal node is added, the internal area of the cell increases as nodes readjust to achieve their new equilibrium arrangement. As the internal area of a cell increases, the cell wall will stretch. When the cell wall becomes stretched enough that the distance between two successive cell wall nodes passes the membrane threshold length, Linear_{thresh} (See Table 3.2), a new cell wall node is added. This is how cell wall elongation is achieved.

The addition of new cell wall nodes in the model represents the addition of new cell wall material in the biological system. When stretched above a certain threshold, the pectin cross-links in the cell wall break and the insertion of new cell wall material results in the irreversible expansion of the cell wall. The addition of new cell wall material and formation of new pectin cross-links allows cells to increase their size without compromising strength of the cell wall. Thus, modeling growth as elastic stretching combined with the addition of new cell wall material is a biologically-relevant component of our model since wall expansion due to turgor pressure is accompanied by the synthesis and integration of new wall material [24, 25, 111, 59].

In addition, since nodes function as a coarse-grained representation of cell wall material, new nodes are added in simulations to maintain the resolution scale (See section 3.2.7). Representation of the two primary cell wall regions on either side of the middle

lamella is also a biologically relevant component of our model since contribution of new cell wall material during expansion is carried out independently by neighboring cells, and the orientation and rate of microfibril deposition can vary between adjacent cells [121]. Moreover, individual cell wall mechanical parameters including extensibility and mechanical stiffness play an important role in determining the rate of cell expansion, the main axis of expansion of a cell, and consequently the degree of growth anisotropy. How individual cells regulate these parameters is fundamental to understanding how plants control global tissue patterns [20, 34, 54].

In the SAMs of *Arabidopsis*, the main axis of expansion of cells varies between the different cell layers likely due to differences in anisotropic cell wall properties. In our model, rotational spring parameters, k_{bend} and θ_{eq} regulate cell expansion directions by controlling the degree of bending between cell wall segments along each axis. To do this, a growth direction vector, d_c, is defined for each cell upon creation and changes as a result of the cell layer, concentration of WUS and concentration of CK. Then, a cell wall direction vector, d_w, is computed for each section of the wall. The cell wall direction vector is defined to be the vector connecting two successive nodes.

Sensitivity analysis was performed for individual cell growth direction to determine how cell shape should change as a function of the bending spring constant (k_{bend}) and equilibrium angle (θ_{eq}). After sensitivity analysis, the parameters for each section of the cell wall is determined as a function of d_c and d_w in the following way

$$k_{linear} = k_{linear}^{min} + k_{linear}^{max}(1 - \cos^2\theta) \tag{3.2}$$

where θ is the angle between the growth direction vector, d_c, and the cell wall direction

vector, d_w, k_{linear}^{min} is the minimum value for the linear spring constant of a cell wall section, and k_{linear}^{max} is the maximum linear spring constant of a cell wall section (See Table 3.2). Cell wall segments assigned lower linear spring constants will stretch apart more easily, facilitating faster expansion in the direction parallel the growth direction vector for that cell.

3.2.4 Cell Division

Experimentally tracking division plane orientation along with maximal tensile stress in cell walls and level of biochemical signaling is difficult, especially in cells that are located in the deeper layers of the SAM. For this reason, we model several possible mechanisms driving the positioning of the new cell wall during cell division. Cell division in simulations occurs once the number of internal nodes has doubled. Two spots on opposite sides of the cell wall are chosen and the cell division plane is then determined as the plane that goes through the cells' center of mass and connects these two spots on the wall. The cell is then divided by a straight line created from a set of new cell wall nodes. After division, parameters for nodes of each individual daughter cell are inherited from the divided cell, and each daughter cell starts with half the amount of cytoplasm that was in the divided cell.

Division plane orientation in simulations is determined based on several possible mechanisms. The cell will determine the position of the new cell wall according to tensile stress in its cell wall, according to its concentration of CK signaling, or a combination of both the mechanical and biochemical signals it's experiencing. Division plane orientation based on maximum tensile stress in the cell wall only is determined by choosing the two

pairs of adjacent cell wall nodes that are furthest apart since these are the spots where the cell wall is under highest tensile stress.

Alternatively, division plane orientation based on chemical signaling only is determined by the level of CK concentration in the cell. Cells with CK concentration above a certain threshold will divide periclinally regardless of mechanical stress on the cell wall. Both mechanisms for division will be tested in future simulations to determine the relative contribution of mechanical stress and CK concentration in determining division plane orientation. The effect of division plane orientation on morphological features such as cell growth direction and curvature of the L1 layer of the SAM will be compared against experimental images and used to determine the contribution of each type of signal in determining division plane orientation.

3.2.5 Equations of Motion

The potential functions described above are used in the model equations to calculate the displacement of each internal or cell wall node at each time step based on their interactions with neighboring nodes resulting in the deformation of cells within the tissue. A complete list of all potential functions, parameters, and their biological relevance are provided in Table 3.1 and Table 3.2. We assume that the nodes are in an overdamped regime so that inertia forces acting on the nodes are neglected [36, 57, 80]. This leads to the following two equations of motion describing the movement of internal nodes and cell wall nodes respectively:

$$\eta \dot{x}_i^I = -\left(\sum_j \nabla E_{ij}^{IW} + \sum_m \nabla E_{im}^{II} \right) \tag{3.3}$$

$$\eta \dot{x}_j^W = -\left(\sum_i \nabla E_{ij}^{IW} + \sum_k \nabla E_{kj}^{WWS} + \sum_l \nabla E_{lj}^{WWD} + \nabla E_j^{Adh} \right) \tag{3.4}$$

where $i = 1, 2, ..., N^I$ represent all internal nodes and $j = 1, 2, ..., N^W$ represent all cell wall nodes. η is the damping coefficient, x_i^I and x_j^W are positions of internal nodes and cell wall nodes indicated by indices i and j respectively, m is the index for any internal node interacting with internal node i, k is the index for any cell wall node of the same cell interacting with cell wall node j, and l is the index for any cell wall node of a different cell interacting with the cell wall node j. The two equations above are solved at the same time for all internal and cell wall nodes.

The two equations are discretized in time using the forward Euler method and positions of nodes x_i^I and x_j^W are incremented at discrete times as follows:

$$x_i^I(t + \Delta t) = x_i^I(t) - \left(\sum_j \nabla E_{ij}^{IW}(t) + \sum_m \nabla E_{im}^{II}(t) \right) \frac{\Delta t}{\eta} \tag{3.5}$$

where Δt is the time step size. The same discretization technique is used for the equations of motion of the cell wall nodes.

3.2.6 Model Components at Different Scales

Our model is multi-scale in space and combines four different scales for modeling growth of the meristem. Molecular level descriptions include cell-cell adhesion achieved through coarse-grained approximation of pectin cross-linking in the middle lamella and growth rate determined by WUS concentration of each cell (See section 3.2.8). Sub-cellular level descriptions include separate node representations of the mechanical properties of individual sub-cellular components of the cell wall resulting in detailed simulation of cell growth

Potential Function	**Parameter**	**Value**
E^{II}	U^{II}	75 $nN.\mu m$
	W^{II}	6.71 $nN.\mu m$
	ξ^{II}	0.8 $nN.\mu m$
	γ^{II}	1.34 $nN.\mu m$
E^{IW}	U^{IW}	45 $nN.\mu m$
	W^{IW}	0 $nN.\mu m$
	ξ^{IW}	0.3 $nN.\mu m$
	γ^{IW}	0 $nN.\mu m$
E^{WWD}	U^{WWD}	3.9 $nN.\mu m$
	W^{WWD}	0 $nN.\mu m$
	ξ^{WWD}	0.5 $nN.\mu m$
	γ^{WWD}	0 $nN.\mu m$
E^{Adh}	k^{Adh}	20 $nN.\mu m$
	L^{Adh}	0.8 μm
	Adh_{thresh}	2 μm
E^{WWS}	k_{linear}	150-800 $nN.\mu m$
	k_{min}	150 $nN.\mu m$
	k_{max}	500 $nN.\mu m$
	x_{eq}	0.07 μm
	k_{bend}	12 $nN.\mu m$
	θ_{eq}	circle
	Linear_{thresh}	.15 μm
	η_{stem}	3
	η_{normal}	1
	Initial number of internal nodes	15
	Initial number of cell wall nodes	150
	Time step	0.003

Table 3.2: Parameter values used in simulations

and anisotropic cell wall expansion and sub-cellular representation of increase in cytoplasmic pressure to generate turgor pressure resulting in detailed simulation of interaction of cytoplasm and cell wall.

Cell level descriptions include detailed description of individual cell behavior including determination of the cell growth direction and interactions of neighboring cells modeled through modification and structural reorganization of the cell wall and cell-cell adhesion. Descriptions of behavior at the multicellular, tissue level include response of the tissue to non-homogeneous distribution of WUS protein, multicellular interactions between the three different cell layers that lead to shape and size of the meristem (See section 5.2.1 and 5.2.2) and model provides a detailed description of stresses in tissue (See section 5.2.3).

3.2.7 Coarse Graining Approach

In our simulations, the number of nodes used to represent each cell is chosen based on the desired level of coarse graining representation. Then, Morse potential parameters are calibrated based on the average size of cells determined from experimental images (Figure 3.4). Next, the number of cell wall nodes is chosen to make sure volume exclusion is satisfied. Finally, we wanted the minimum number of elements that met these criteria for computational considerations. Cell wall nodes in the beginning of a simulation are arranged in a circle for each cell, and internal nodes are randomly placed within each cell. After initialization, internal nodes rearrange and cells attain biological shapes, similar to the experimentally observed cell shapes in the SAM (Figure 5.1). Cells in a simulation constantly grow and interact with each other resulting in a detailed dynamic representation

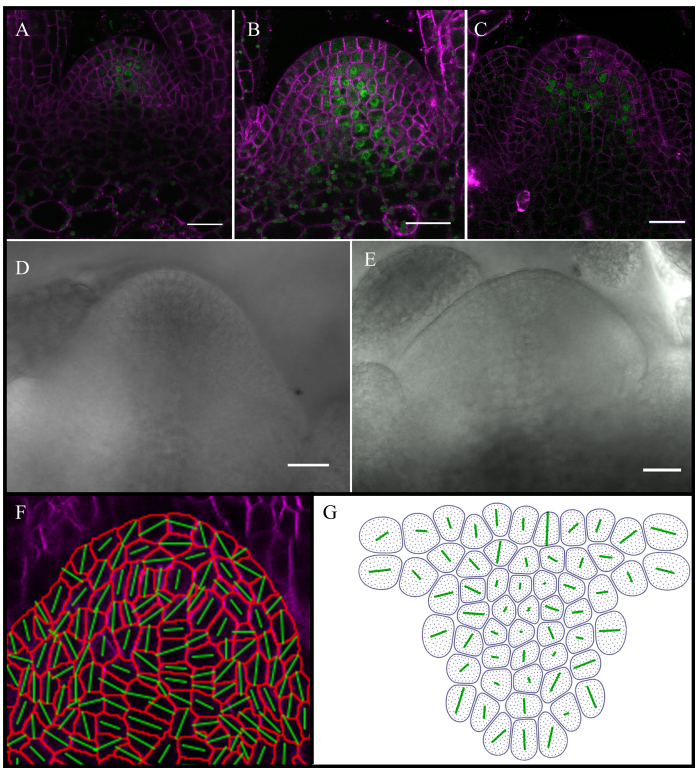

Figure 3.4: Experimental images from wildtype and four alternative systems and application of the image quantification methods. (A) Wildtype SAM showing WUS accumulation in green. Reprinted with permission from [113]. (B) Meristem experiencing the ectopic over-activation of CK signaling in the CZ for 12 hours. Increased WUS accumulation shown in green. Reprinted with permission from [113].(C) *clv3-2* null mutants obtained by our group. (D) Ectopic activation of eGFP-WUS from the CZ-specific *CLV3* promoter. Reprinted with permission from [89]. (E) Misexpressed eGFP-WUS form, in the CZ, that is tagged with a potent nuclear localization signal (nls-eGFP-WUS). Reprinted with permission from [89]. (F-G) Main axis of expansion of cells in wildtype SAM from experiments (F) and simulations (G). Green bars depict the main axis of expansion calculated for each cell. Scale bars are 20μm.

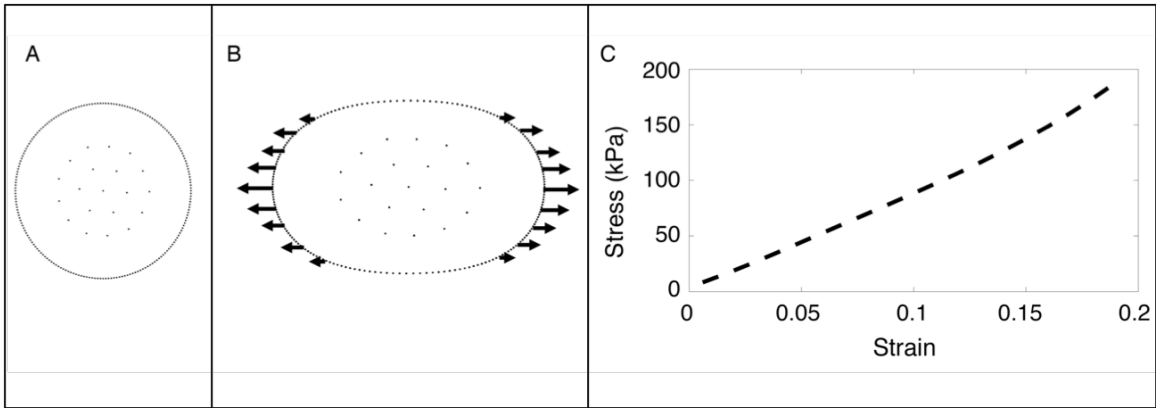

Figure 3.5: Calibration of model parameters. (A-B) Calibration test to determine parameters for cell elasticity. (A) Cell at equilibrium with no force applied. (B) Cell has deformed after linearly increasing force is applied to nodes on both sides. (C) Stress versus strain graph for single cell calibration of modulus of elasticity.

of the combined growth of the L1, L2 and deeper L3 layers of the SAM tissue.

3.2.8 Model Assumptions and Calibration

Mechanical Properties of Individual Cells

Model parameters representing cell wall mechanical properties were calibrated using biophysical measurements from a large body of literature [for reviews see 41, 97]. Model parameters determining the spatial distribution of WUS in simulations were calibrated using experimental data obtained by our group.

Cell wall mechanical stiffness was calibrated using experimentally measured modulus of elasticity (E) of a single cell. Several different experiments have been performed to determine biological ranges for E in plants [97]. In model simulations, the modulus of

elasticity is determined by applying a linearly increasing force to cell wall nodes on both sides of a cell and calculating the cell's deformation (Figure 3.5A-B). The slope of the graph of the stress versus strain curve provides the elasticity of the cell (Figure 3.5C). We have chosen values for k_{bend} and k_{linear} so that E lies within the biological range of $(.1 - 1)$ MPa measured for plant cells [41].

Cell Growth Rates

The spatial confinement of WUS to an exact domain within the SAM was shown to be crucial for maintaining a constant number of stem cells over time [131]. In the model, the WUS density distribution is created by assigning each cell an average concentration of WUS determined as follows. Experimental images of 13 different meristems were used to derive a function for the average WUS concentration of each individual cell based on the distance from its cell center to the RM where *WUS* is expressed (Figure 3.6A).

This data was fit to an exponential function because WUS quantification from experiments suggests that the WUS protein distribution is exponentially distributed (Figure 3.6A). *WUS* is expressed in a few cells of the rib meristem (RM) called the niche/Organizing Center (OC) located just beneath the CZ and migrates from the RM into adjacent cells. Since the distribution of the WUS signal from experiments is exponential, and WUS signaling dynamics have been previously modeled using reaction-diffusion equations [50, 130], we chose to fit an exponential function to the experimental data. This resulted in the following concentration of WUS for an individual cell:

$$WUS(x) = 109.6 * \exp(-0.1135 * x) + 27.69 * \exp(-0.003414 * x) \tag{3.6}$$

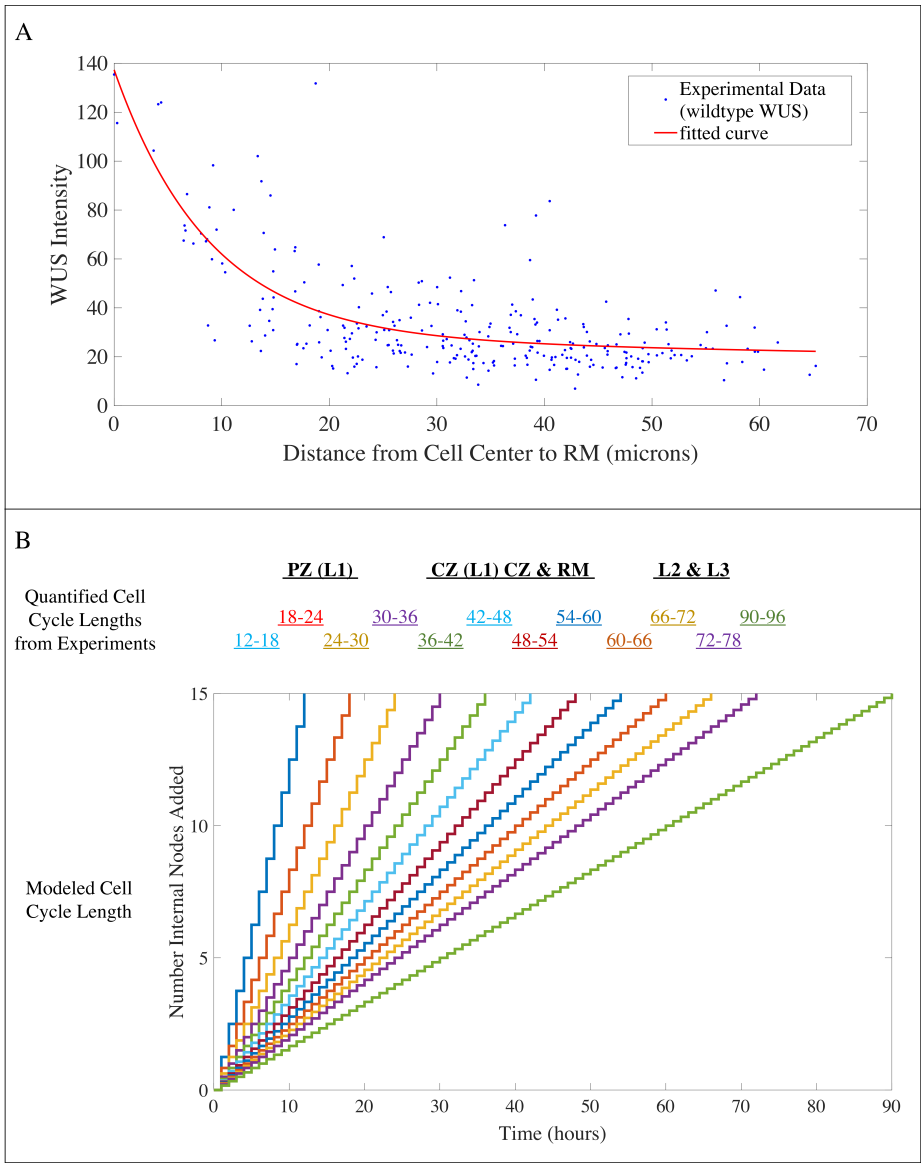

Figure 3.6: (A) Graph showing the levels of WUS protein distribution in space. The WUS levels in different cells are plotted as a function of the distance from the RM. Blue dots represent experimentally quantified WUS levels. Red line represents the fitted curve from equation 3.6. (B) Graph showing the frequency of addition of internal nodes based on cell cycle length. Cell growth rates are assumed to be directly correlated to the cell cycle length derived from experimental observations in an earlier study (Reddy et al., 2004).

WUS Intensity	**Cell Cycle Length**
WUS $\leq$ 12	12-18 hours
12 $<$ WUS $\leq$ 24	18-24 hours
24 $<$ WUS $\leq$ 36	24-30 hours
36 $<$ WUS $\leq$ 48	30-36 hours
48 $<$ WUS $\leq$ 60	36-42 hours
60 $<$ WUS $\leq$ 72	42-48 hours
72 $<$ WUS $\leq$ 84	48-54 hours
84 $<$ WUS $\leq$ 96	54-60 hours
96$<$ WUS $\leq$ 108	60-66 hours
108$<$ WUS $\leq$ 120	66-72 hours
120$<$ WUS $\leq$ 132	72-78 hours
132 $<$ WUS	90-96 hours

Table 3.3: Cell cycle length as a function of WUS intensity. Data taken with permission from Reddy et al. [92].

where x is the distance from the cell center to the RM where *WUS* is expressed.

The growth rate of each cell is determined in the model by its WUS concentration (See Table 3.3). Several experimental observations suggest that higher levels of WUS may inhibit cell growth and lower levels promote cell growth [92]. These observations show that: a) WUS protein accumulates at higher levels in the slow growing RM and the CZ, and at lower levels in the fast growing PZ; b) ectopic activation of WUS outside the RM destabilizes WUS leading to a lower accumulation and increased growth rates; c) ectopic overexpression of a nuclear-enriched form of WUS leads to highly irregular SAMs which could be due to local differences in WUS concentration that in turn inhibit or stimulate growth in adjacent cells/regions [89, 113, 131]. Therefore, we assume in the model that cells with the lowest concentration of WUS have the highest growth rate and cells with the highest concentration of WUS have the lowest growth rate (Figure 3.6B and Table 3.3).

Boundary Conditions

There is only one boundary condition imposed during simulations. The bottom most layer of cells in the deeper L3 layers has a higher damping coefficient and subsequently this layer of cells acts as a barrier the same way the cells of the stem would in the biological system (Table 3.2). Other cells in the tissue move and fluctuate freely as cells grow and interact. WUS concentration of each cell is initially determined by Eq. 3.6 (Figure 3.6A and section 3.2.8) based on the location of the center of each cell. Since we assume a steady-state distribution of WUS, once the WUS signaling domain is set up upon initiation of the tissue, the WUS concentration of each cell is not updated and therefore the WUS signaling domain will also move and fluctuate freely as cells grow and interact.

Timescale

In an unperturbed system, spatial domains of chemical signaling remain unchanged and balanced by underlying feedback mechanisms [93]. Thus, in our model, we assume that steady-state, spatial distribution of WUS is maintained over the simulation time period and therefore we do not take into account transcription factor and protein movement explicitly. In plants treated with ectopic activation of CK signaling, obvious changes in the size of the WUS signaling domain and shape of the meristem occurred by 22 hours after treatment [113]. For this reason, the time period of 20 hours for simulations was chosen because it was long enough to observe the impact of signaling changes on cell growth rates as well as determine how these changes translate into changes in tissue morphology.

Cell proliferation rates and division plane orientation affect both the shape and size

of individual cells as well as topology of the tissue. Coordinated division plane orientation and expansion of cells as a mechanism for determining shape of the tissue is especially important in plants since cells do not rearrange. In addition, creation of new cell walls leads to local reinforcement of the tissue altering mechanical properties of the tissue in a preferential direction. However, the position of the new cell wall is ultimately determined by the preprophase band (PPB), a ring structure formed by cortical microtubules before the cell enters mitosis.

Previous experimental studies suggest that cortical microtubules orient according to the maximal mechanical stress direction which is largely determined by tissue shape [45, 102, 103, 121, 125]. This suggests that cortical microtubules serve as intermediates between tension patterns in the tissue in cell walls and cell division plane orientation. Thus, distribution of stress throughout the tissue provides supracellular cues that play a role in determining division plane orientation of individual cells.

For this reason, simulations in this paper do not include division. Simulations in this paper test mechanisms for SAM growth based on the combined contribution of mechanical properties of sub-cellular components of individual cells via anisotropic cell growth directions and varied cell growth rates based on WUS concentration and predict how these specific mechanisms establish the distribution of stress throughout the tissue. In order to run simulations that quantify the relative contributions of chemical versus mechanical signaling in determining division plane orientation, it is necessary to first gain biological insights about individual cell mechanisms for anisotropic cell expansion as well as mechanical interactions between neighboring cells before new cells are added to the tissue.

Future simulations will encompass a larger timescale and include cell division to predict new mechanisms for SAM development that quantify relative contributions of chemical versus mechanical signaling in determining division plane orientation. The extended model will provide a platform for testing the feedback between mechanical properties of the tissue that contribute to cell division orientation patterns and cell division orientation patterns that affect mechanical properties of the tissue.

Chapter 4

Sensitivity Analysis and Computational Implementation of the Model

4.1 Sensitivity Analysis

Mathematical and computational models of real-world biological systems are made up of many different equations formulated based on a specific set of assumptions. Sensitivity Analysis (SA) refers to a collection of mathematical techniques designed to quantify how variation in model outputs may be attributed to model inputs (i.e., parameters, initial conditions, etc.). For biological applications, parameters can be estimated using experimental data if available, but a central question is what should be done when parameter values cannot be properly estimated due to incomplete, ambiguous, contradictory exper-

imental data or even a lack of current experimental techniques to measure the property of interest. SA has a number of useful purposes including model corroboration, research prioritization, model simplification, identifying critical or interesting regions in the space of the input factors, and parameter estimation [100]. For example, sensitivity analysis can be used to identify which input parameters are most important in contributing to the prediction imprecision of the outcome variable. In addition, input parameters can be ranked by their importance allowing for optimization procedures that produce better input parameter estimates.

4.1.1 Local Sensitivity Analysis

One of the most straightforward methods for completing sensitivity analysis is to vary each model input parameter one at a time (OAT) while other input parameters remain fixed. OAT methods and the majority of other SA techniques found in the literature are based on derivatives [100, 65]. In these methods, importance is assigned to input factors by their impact on the approximate derivatives of outputs with respect to a change in the input. For example, the mathematical definition of the sensitivity of an output Y_j versus an input X_i can be defined in terms of derivatives as $\partial Y_j / \partial X_i$. OAT and other derivative-based methods have the advantage that they are very simple and can be computationally quick if only a small number of input parameters are being tested. However, they only provide information about the system that is inherently local since they do not study the impact of varying multiple parameters at the same time and only a small region of parameter space can be explored [100, 65]. Local approaches can be informative if there is little uncertainty in model input parameters or if it is known that there is little interaction between input

parameters [100].

4.1.2 Global Sensitivity Analysis

In biology, input factors are often very uncertain and therefore local SA techniques are not appropriate for a quantitative analysis since the possibility of important factors being overlooked or critical combinations of input factors being neglected is high due to a lack of thorough exploration of the space of input factors [37]. Global sensitivity analysis (GSA) methods consider the change in model outputs as input parameters are varied simultaneously over specified ranges [100, 65]. GSA methods can require more computational work than local methods, but they have the added advantage that they can uncover relationships between multiple input parameters and highlight nonlinear variable responses. GSA methods are often probabilistic in nature. More specifically, they consider the underlying system output to be a random variable over a probability space of parameter inputs, and quantify the sensitivity of a model output by its variance. In these approaches, the variance in model output is decomposed to attribute fractions of the variance to individual model inputs and also groups of model inputs.

One common approach to sensitivity analysis is to use a full factorial experimental design [100]. This design consists of two or more factors that are set to k different levels and all possible combinations are tested. This sampling design has the advantage that the whole parameter space can be explored by generating factorial designs with many levels for each parameter. In general, k parameters would require s^k simulations to generate all combinations for a k-level factorial design. However, because of the explosive growth of the quantity s^k, two-level designs are typically used where all combinations of the highest

and lowest parameter values are tested. With only two levels there is no way to measure changes in small variations of each parameter within the domain and as a result two-level factorial designs often only pick up linear effects.

A more sophisticated and efficient sampling technique that allows for the simultaneous variation of all model input parameters is Latin Hypercube Sampling (LHS) [65]. The LHS scheme is an extremely efficient sampling design proposed by McKay, Conover and Beckman [68]. LHS belongs to the Monte Carlo class of sampling methods. This method produces an unbiased estimate of the average model output and requires fewer samples than simple random sampling to achieve the same accuracy. More specifically, LHS is a stratified sampling without replacement technique, where the random parameter distributions are divided into N equal probability intervals, which are then sampled. N represents the sample size. The choice for N should be at least $k+1$, where k is the number of parameters varied, but usually the choice for N should be much larger to ensure accuracy. A sensitivity analysis may then be performed by calculating partial rank correlation coefficients (PRCC) for each input parameter and each outcome variable.

The sampling is done by randomly selecting values from the pdf of each parameter of interest. Each interval for each parameter is sampled exactly once (without replacement), so that the entire range for each parameter is explored. A matrix is generated that is commonly called the LHS matrix that consists of N rows for the number of simulations and of k columns corresponding to the number of varied parameters. N model solutions are then simulated, using each combination of parameter values, ie.e each row of the LHS matrix. The model output of interest is collected for each model simulation and different

model outputs can be studied if more than one model output is of interest.

4.1.3 Methodology

The LHS followed by PRCC technique involves seven steps. They are as follows.

Step one. Identify parameters of interest and define probability distribution functions for parameters.

In our model, linear-spring interactions given by the following equation $E_{linear} = \frac{1}{2}k_{linear}(x-x_{eq})^2$ are defined between adjacent nodes of the cell wall to maintain the length of cell wall segments and regulate cell wall extensibility. Rotational spring interactions defined between three successive nodes of the cell wall are described by the following equation, $E_{bend} = \frac{1}{2}k_{bend}(\theta-\theta_{eq})^2$ and are used to maintain a prescribed degree of bending between cell wall segments (Bathe and Saunders 1984). The degree of bending between cell wall segments represents the level of alignment and coordinated orientation of the cellulose microfibrils.

Bending stiffness in the model limits cell expansion along the axis perpendicular to the preferred growth direction similar to how cells lay down microfibrils to limit expansion in experimental observations. The way this is achieved is by assigning each node its θ_{eq} value based on its location within the cell. Nodes whose location is within the region of the cell wall perpendicular to the preferred growth direction are assigned an equilibrium angle of 180 degrees. All other nodes are assigned a circular equilibrium angle. In this way the parameter k_{bend} is split into two separate parameters, $k_{bend_{high}}$ and $k_{bend_{low}}$. $k_{bend_{high}}$ is the bending spring coefficient for nodes in the region of the cell wall where θ_{eq} is set to 180 degrees, and $k_{bend_{low}}$ is the bending spring coefficient for all other nodes.

Ranges for the parameters k_{bend} and k_{linear} are determined using elastic modulus

of cells measured in experiments. However, sensitivity analysis techniques are necessary to determine the relationships between each of these parameters and three important cell shape characteristics, area, ratio of longest axis to shortest axis and dynamic curvature. The probability distribution function assigned for each parameter was the uniform distribution.

Step two. Calculate the number of simulations (N).

The LHS sampling technique involves sampling without replacement. This mean that if K draws are to be made, where K equals the number of uncertain variables, the Kth draw would be predetermined. This, the lower limit value of N, where N equals the number of simulations, should be at least $K + 1$. There is no exact rule for determining the adequate sample size for the LHS scheme. The appropriate sample size for a specific analysis should also take into account the desired significance level for the partial rank correlation coefficient. In the present analysis K is equal to 3 and N was set to 20.

Step three. Divide the range of each of the K parameters into N equally probable intervals.

Step four. Create the LHS table.

The LHS scheme involves random sampling without replacement. Each equally probable interval for each input parameter is sampled once. An LHS table is generated as a matrix where N is the number of simulations and K is the number of sampled input parameters. N sampling indices of the first variable are paired randomly with N sampling indices of the second variable and the random pairing continues until all K input variables are included and the $N \times K$ matrix has been generated.

Step five. Sample the values of the input parameters.

Step six. Analysis of model outcomes: Uncertainty analysis.

The results of the simulation runs consist of N observations of the three outcome variables area, ratio of longest to shortest axis and dynamic curvature. Distribution functions for each of the outcome variables can be directly derived and characterized by simple descriptive statistics since the N observations correspond to a range of probable outcomes rather than the absolute upper and lower bounds of the system. Descriptive statistics provide a measurement of the variability in the outcome variable due to the estimated parameters.

The LHS uncertainty technique was used to explore the effect of uncertainty in $k_{bend_{high}}$, $k_{bend_{low}}$ and k_{linear} on the prediction precision of two outcome variables: cell area and ratio of shortest to longest axis. Descriptive statistics for these distributions are given in Table 4.1.

Step seven. Analysis of model outcomes: Sensitivity analysis.

The N observations of each outcome variable from simulations can be used to assess the sensitivity of the outcome variables to the estimation uncertainty in the input parameters. In the LHS scheme all of the parameters are varied simultaneously. Since the input parameters are often interdependent PRCC should be used to evaluate statistical relationships. Calculation of PRCC enables the determination of the statistical relationships between each input parameter and each outcome variable while keeping all of the other input parameters constant at their expected value. This procedure enables the independent effects of each parameter to be determined, even when the parameters are correlated. A PRCC

	AREA	RATIO
MIN	119.635	0.5142
MAX	351.8957	0.9976
MEAN	202.2367	0.7461
MEDIAN	176.9506	0.6750
VARIANCE	4.99e+03	0.0384

Table 4.1: Descriptive statistics for uncertainty in two outcome variables, cell area and ratio of shortest to longest axis of cells.

indicates the degree of monotonicity between a specific input variable and a particular outcome variable. Therefore, only outcome variables that are monotonically related to the input parameters should be chosen for this analysis. The sign of the PRCC indicates the qualitative relationship between each input variable and each output variable. The magnitude of the PRCC indicates the importance of the uncertainty in estimating the value of the input variable in contributing to the imprecision in predicting the value of the outcome variable. The relative importance of the input variables can be directly evaluated by comparing the values of PRCC.

A suggested starting point in sensitivity analysis using sampling-based methods is to examine scatter plots. Scatter plots enable graphic detection of nonlinearities, non-monotonicities, and correlations between model inputs and outputs. Scatter plots (Figure 4.1) indicate there there is a linear relationship between Area and k_{linear} and in addition there is a linear relationship between Ratio and $k_{bend_{high}}$.

Next, the MATLAB function, *stepwiselm*, was used to perform stepwise regression to remove insignificant terms from the model (See Table 4.2 and Table 4.3 for details).

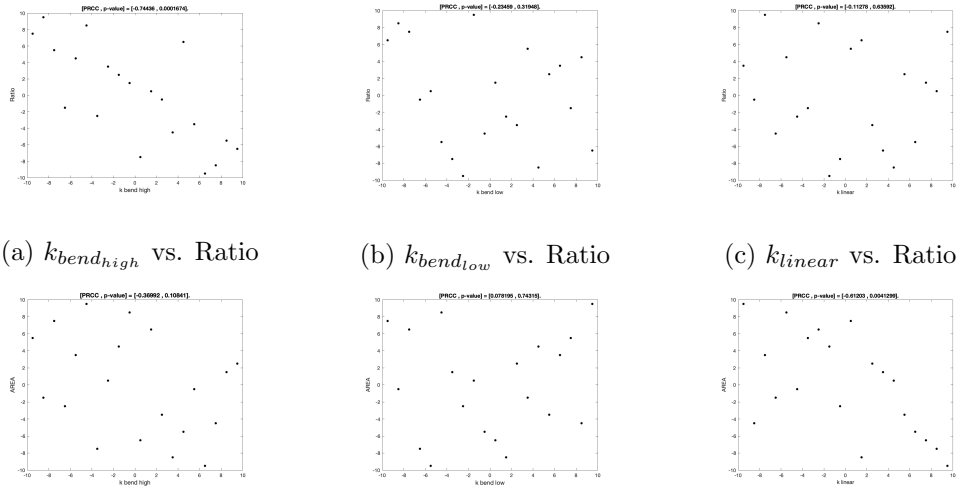

(a) $k_{bend_{high}}$ vs. Ratio (b) $k_{bend_{low}}$ vs. Ratio (c) k_{linear} vs. Ratio

(d) $k_{bend_{high}}$ vs. Area (e) $k_{bend_{low}}$ vs. Area (f) k_{linear} vs. Area

Figure 4.1: Scatterplot graphs for influence of input variables on two outcome variables, cell area and ratio of shortest to longest axis.

	Estimate	**SE**	**tStat**	**pValue**
Intercept	296.61	24.704	12.006	5.0029e-10
k_linear	-0.23925	0.055581	-4.3044	4.2687e-4
R-squared:	0.507	**Adjusted R-Squared:**	0.48	
F-statistic:	18.5	**p-value:**	4.27e-4	

Table 4.2: Summary of reduced regression model for cell area

The term with the largest p-value was iteratively removed from the model, and the model was refit. This was done until an F-test for change in the sum of squared error returned a p-value below α, which was set to be determined based on the impact on the adjusted R^2 of the model (Table 4.2 and Table 4.3 for details). The term with the largest p-value was iteratively removed from the model, and the model was refit. The outcome was the

	Estimate	SE	tStat	pValue
Intercept	0.974	0.067	14.537	2.1755e-11
k_bend_high	-0.00755	0.0019273	-3.9167	0.001011
R-squared:	0.46	**Adjusted R-Squared:**	0.43	
F-statistic:	15.3	**p-value:**	0.00101	

Table 4.3: Summary of reduced regression model for ratio of shortest to longest axis of cells

following two equations for area and ratio as a function of k_{linear} and $k_{bend_{high}}$ respectively.

$$\text{Area} = -23925 * k_{linear} + 296.61 \tag{4.1}$$

$$\text{Ratios} = -0.00755 * k_{bend_{high}} + 0.97444 \tag{4.2}$$

4.2 Computational Implementation

The code for this work was implemented in C++ using OpenMP for parallelization. A flowchart outlining the computational implementation of the model is given in the Appendix [1].

[1]The code is available at `https://github.com/mikahlbk` in the folder ScePlantCells_Parallel

Chapter 5

Results

5.1 Experimental and Image Analysis Results

Experimental Methods

Side view experimental images of sectioned SAMs were obtained by confocal microscopy [113]. SAMs were imaged using a fusion protein of eGFP-WUS to track WUS accumulation [113, 130]. In addition, plasma membrane staining was used to provide a proxy for visualization of individual cell walls [113]. Wildtype plants used for model validation were grown under normal conditions. To study spatial manipulation of WUS levels, four systems were employed:

1) A recent study has shown that CK signaling stabilizes the WUS protein in the deeper L3 layers of the RM [113]. To induce cytokinin response in cells of the L1 and the L2 layers, active TypeB ARABIDOPSIS RESPONSE REGULATOR1 (ARR1), a transcription factor that functions downstream of the CK receptors, was constitutively

misexpressed in dexamethasone inducible fashion, by using the *CLV3* promoter [For further details see 113]. For this experiment, ectopic activation of CK signaling in the outer layers leads to an increase in the diameter of the WUS signaling domain as well as increased WUS accumulation in the meristem that spreads out into the deeper layers, and modestly into the L1 or L2 layers (Figure 3.4B) [113].

2) Ectopic activation of eGFP-WUS from the CZ-specific *CLV3* promoter leads to uniformly lower WUS accumulation in all cell layers of highly enlarged and much taller SAMs [131, 89] (Figure 3.4 D).

3) To achieve higher levels of nuclear WUS, we utilized data sets from an earlier study which misexpressed an eGFP-WUS form, in the CZ, that is tagged with a potent nuclear localization signal (nls-eGFP-WUS) (Figure 3.4 E). For further details see figure 5C and F in Perales et al. 2016. In this condition, higher nuclear WUS was detected in patches of cells in highly irregularly shaped and much flatter SAMs.

4) WUS accumulation was followed in *clv3-2* null mutants which accumulate WUS at much higher levels in the nuclei of L2 and deeper L3 layers and extremely low levels in the nuclei of the L1 layer (Figure 3.4 C) [89].

Image analysis

Analysis and quantification of the WUS signal was performed using a combination of ImageJ and the HK-means and Active contour packages within the ICY bio-image analysis software [113]. Plasma membrane staining makes it possible to distinguish between the cell outlines of individual cells and thus measure the amount of signal in each

cell as well as describe other cell characteristics such as cell center and the main axis of expansion for each cell.

The main axis of expansion of cells in both experimental images and simulations is quantified for comparison and model validation. For *in vivo* cells, the main axis of expansion is inferred from cell shapes observed from single-time-point images. First, images are segmented in ImageJ. Next, the EpiTools image processing software [47] is used to fit an ellipse to each individual cell contour and extract the angle and magnitude of the longest axis of the ellipse. The angle and magnitude pair are then used to define the main axis of expansion for each cell in the modeling domain (Figure 3.4F). For simulated cells, the expansion direction is calculated similarly to experimental images using resulting cell shapes from the final time step of each simulation (Figure 3.4G).

Curvature of the L1 layer of the SAM in both experiments and simulations is quantified for comparison and model validation. For both experimental and simulation images, the center of each cell in the L1 layer is recorded and a circle is fit to the resulting set of data points using the Circle Fit (Pratt method) in matlab [66] (See SI 1.1). The radius of the fitted circle is used as a metric to compare curvature of the L1 layer of the SAM in simulations versus experiments.

5.2 Model Simulation Results

5.2.1 Mechanisms Determining Overall Shape of the SAM

The computational model was used to study morphological implications of individual cell behaviors in the SAM by simulating combined growth of the L1, L2, and deeper

L3 layers (See [5] for details). Model simulations were run to determine whether layer dependent mechanical anisotropy at the sub-cellular and cellular level combined with experimentally calibrated diameter of the WUS signaling domain were sufficient to reproduce experimentally observed expansion directions of cells as well as experimentally observed shape and size of the SAM characterized by curvature of the L1 layer (Figure 5.1). In addition, model predictive simulations were run to test the hypothesis that WUS concentration of individual cells controls individual cell growth rates as a mechanism for generating SAM shape and structure.

For simulations of wildtype SAM growth (Figure 5.1A-C), the following assumptions were made. The diameter of the CZ and resulting WUS signaling domain were calibrated using experimental data and described by Eq. 3.6 (Figure 3.6A and section 3.2.8). Cell growth rates were determined based on the WUS concentration of individual cells (See Table 3.3, Figure 3.6B and section 3.2.8). Lastly, cells in the L1 and L2 layers were assigned growth direction vectors parallel to the surface of the SAM and all cells in the deeper layers were assigned growth direction vectors perpendicular to the surface of the SAM.

Tissue shapes obtained in wildtype simulations were compared with tissue shapes observed in experimental images. Namely, the distribution of the angles of the main axis of expansion for all cells in the tissue (See section 5.1) obtained in simulations and experiments were compared to quantify the impact of the expansion direction of individual cells on overall tissue shape (Figure 5.2A-E). A kernel density estimation (KDE) plot for the angle of the main axis of expansion of cells across 13 experimental images was compared to a KDE plot for the angle of the main axis of expansion of cells across 5 simulations. KDE

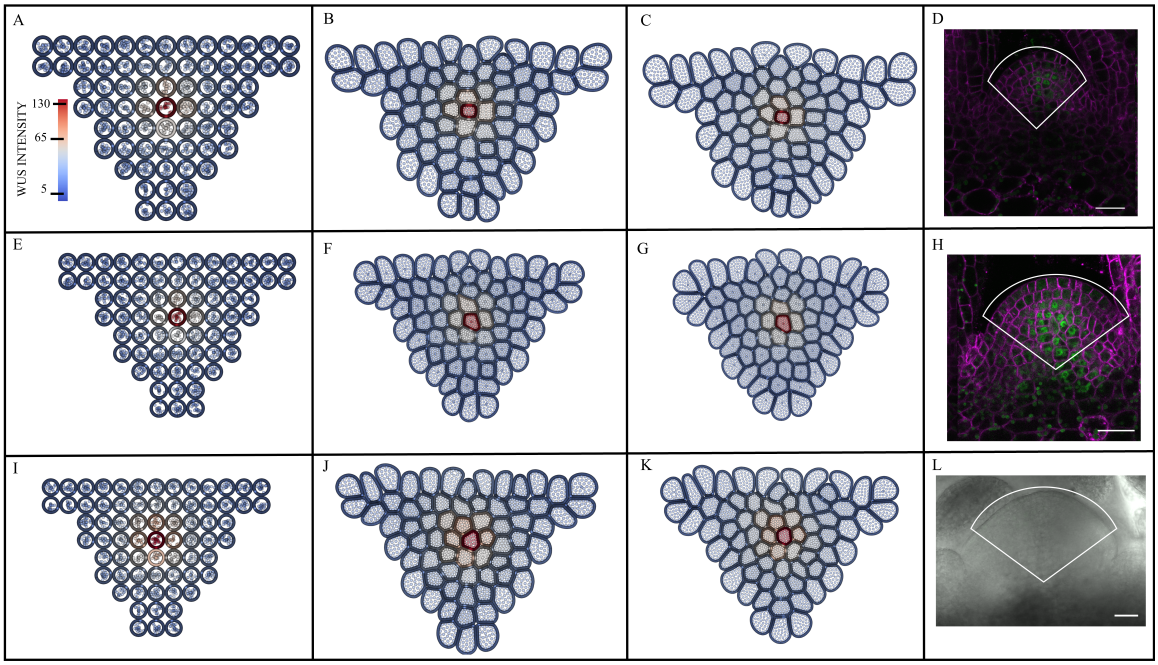

Figure 5.1: Time snapshots of simulations of the formation of the shape and structure of the SAM of *Arabidopsis* and experimental images. (A-C) Simulation of wildtype SAM growth with diameter of CZ equal to 15μm and resulting radius of curvature of the fitted circle to the L1 layer equal to 51.27μm. (D) Experimental image of wildtype SAM obtained by our group. (E-G) Simulation of SAM growth with diameter of CZ equal to 34μm and radius of curvature of the fitted circle to the L1 layer equal to 39.38μm. (H) Experimental image of meristem experiencing the ectopic overactivation of CK signaling in the CZ for 12 hours obtained by our group. (I-K) Simulation of SAM growth with diameter of CZ equal to 56μm and radius of curvature of the fitted circle to the L1 layer equal to 86.42μm. (L) Experimental image of meristem tagged with a potent nuclear localization signal (nls-eGFP-WUS). In (D),(H) and (L) the simulation domain is shown in the enclosed ares in white. Scale bars are 20μm

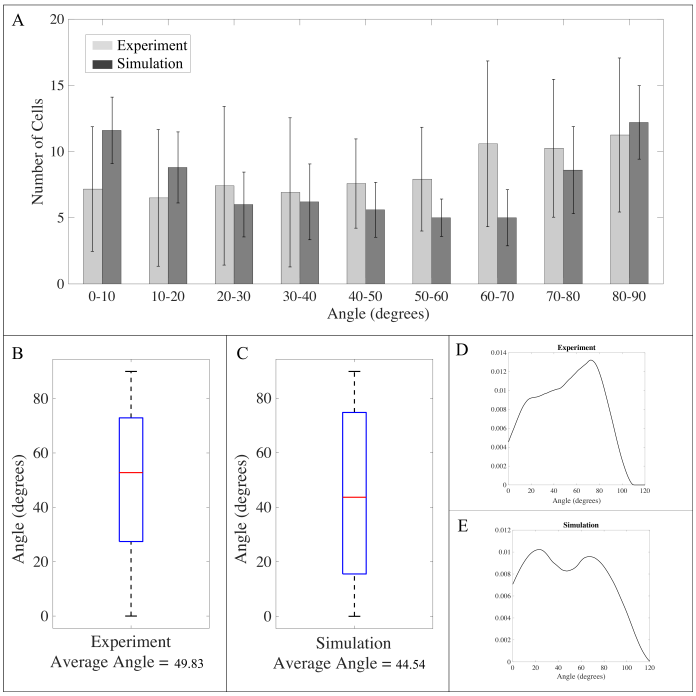

Figure 5.2: Model validation for simulating wildtype tissue growth. (A) Distribution of the angle of the main axis of expansion of cells in experiments versus simulations. Boxplots showing average angle of the main axis of expansion of cells in wildtype experiments (B) and simulations (C). Kernel density estimation (KDE) plots for the angle of the main axis of expansion of cells across experiments (D) and computational simulations (E) respectively. KDE plots demonstrate both data sets follow a bimodal distribution with one mode close to 90 degrees and the other mode close to 0 degrees.

plots demonstrate that both data sets follow a bimodal distribution with one mode close to 90 degrees and the other mode close to 0 degrees. These results are consistent with experimental observations wherein cells in the deeper L3 layers expand perpendicular to the surface of the SAM, i.e. the main axis of expansion is 90 degrees, and cells in the L1 and L2 layers expand parallel to the surface of the SAM, i.e. the main axis of expansion is 0 degrees. Comparison between KDE plots for experimental and simulation data indicate that there was not a significant difference between the two groups. Thus, model assumptions used in the wildtype simulations were enough to reproduce the average angle for the main axis of expansion seen in experimental images.

Lastly, we demonstrated that model simulations reproduced experimentally observed curvature of the L1 layer of the SAM (Figure 5.3). The average radius of curvature of the fitted circle to the L1 layer of the SAM was computed from single-time-point experimental images of 13 different wildtype plants as well as data output from the last time step of 5 wildtype simulations. A t-test comparing the average radius of curvature from wildtype experimental images (50.75 μm) to the average radius of curvature from wildtype simulations (67.19μm) resulted in $p = 0.0656$ demonstrating that there was no significant difference between simulations and experimental data ($\alpha = 0.05$).

5.2.2 Impact of WUS Concentration on Overall Shape of SAM

In addition to quantifying wildtype SAM growth described above, the average curvature of the L1 layer of the SAM was computed from experimental images from 26 ectopic activation of CK experimental meristems (avg = 28.06 μm), 7 ectopic activation of eGFP-WUS experimental meristems (avg = 25.63 μm), 8 *clv3-2* null mutant experimental

meristems (avg = 32.17 μm) and 10 ectopic activation of nls-eGFP-WUS experimental meristems (avg = 86.28μm) (Figure 5.3). A t-test comparing the average curvature of the L1 layer of wildtype meristems to each of the four alternative systems resulted in $p = 3.0230\text{e}-08$, (ectopic activation of CK), $p = 0.0016$ (ectopic activation of eGFP-WUS), $p = 0.0616$ (ectopic activation of nls-eGFP-WUS) and $p = 0.0060$ (*clv3-2* null mutants), respectively. These results demonstrate that ectopic activation of CK meristems, ectopic activation of eGFP-WUS meristems and *clv3-2* null mutants all lead to significant increase in the curvature of the L1 layer of the SAM and ectopic activation of nls-eGFP-WUS meristems are not significantly more curved than wildtype meristems ($\alpha = 0.05$).

To investigate the impact of WUS concentration of individual cells controlling cell growth rates on curvature of the L1 layer, twenty simulations were run with different diameters of the CZ (Figure 5.4). Values for the diameter of the CZ were chosen from the range 15μm - 65μm. This range was used because the average diameter of the CZ in wildtype experimental images is 15μm, and the maximum possible diameter of the CZ for simulations is 65μm. For sampling, the range 15μm - 65μm was divided into twenty intervals and each interval was sampled exactly once (without replacement), so that the entire range for the parameter was explored. Each of the twenty samples was used to generate a different WUS signaling domain for a new simulation (Figure 5.4).

Results demonstrate that the relationship between the diameter of the CZ and radius of curvature of the fitted circle to the L1 layer of the SAM is not linear. Meristems with diameter of the CZ between 32μm and 45μm have the smallest radius of curvature. In addition, once the diameter of the CZ passes 45μm, meristem growth starts to flatten out

and the radius of curvature of the fitted circle to the L1 layer increases. Model predictive simulations demonstrating significant morphological changes due to WUS concentration of individual cells controlling growth rates could be linked to WUS concentration-dependent transcriptional regulation of *CLV3* [89] (See section 6.1 for details). Results from each of the twenty different simulations along with the WUS signaling domain used in each of the twenty different simulations are provided in Figure 5.4. Individual cell growth rates were assigned as before (See section 3.2.8 and Table 3.3) and layer dependent mechanical properties of cells remain the same.

5.2.3 Impact of WUS Concentration on Internal Pressure Distribution in Tissue

The average internal pressure of individual cells across the L1, L2 and deeper L3 layers of the SAM was calculated after 20 hours of growth separately in simulations representing wildtype (diameter of CZ equal to 15μm), increased diameter of CZ (34 μm $\leq$ diameter $\leq$ 44 μm), and uniform cell growth (diameter of CZ equal to 56μm) (Figure 5.5A) simulations. Next, the average internal pressure across the CZ was calculated for each simulation (Figure 5.5B). Results show distinct patterns of pressure accumulation for wildtype (avg = 70.32 kPa), increased diameter of CZ (avg = 72.77 kPa) and uniform cell growth simulations (avg = 80.09 kPa) (Figure 5.5C-E). Stem cells in uniform growth simulations experience higher pressure compared to wildtype and increased diameter of CZ simulations. Model predictive simulation results suggest that distribution of pressure in the

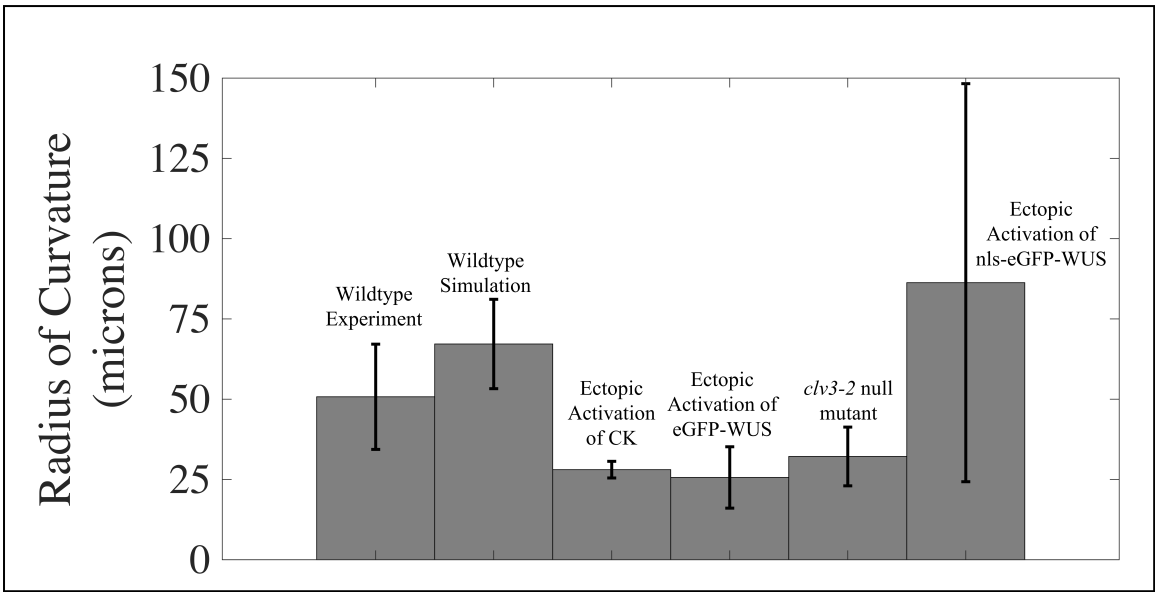

Figure 5.3: Comparison of radii of curvature for wildtype meristems from experiments and simulations and radii of curvature for four alternative systems. Average radius of curvature across 13 wildtype experimental meristems is 50.75 μm, average radius of curvature across 5 wildtype simulations is 67.19 μm, average radius of curvature across 26 ectopic activation of CK experimental meristems is 28.06 μm, average radius of curvature across 7 ectopic activation of eGFP-WUS experimental meristems is 25.63 μm, average radius of curvature across 8 *clv3-2* null mutant experimental meristems is 32.17 μm and average radius of curvature across 10 ectopic activation of nls-eGFP-WUS experimental meristems is 86.28μm.

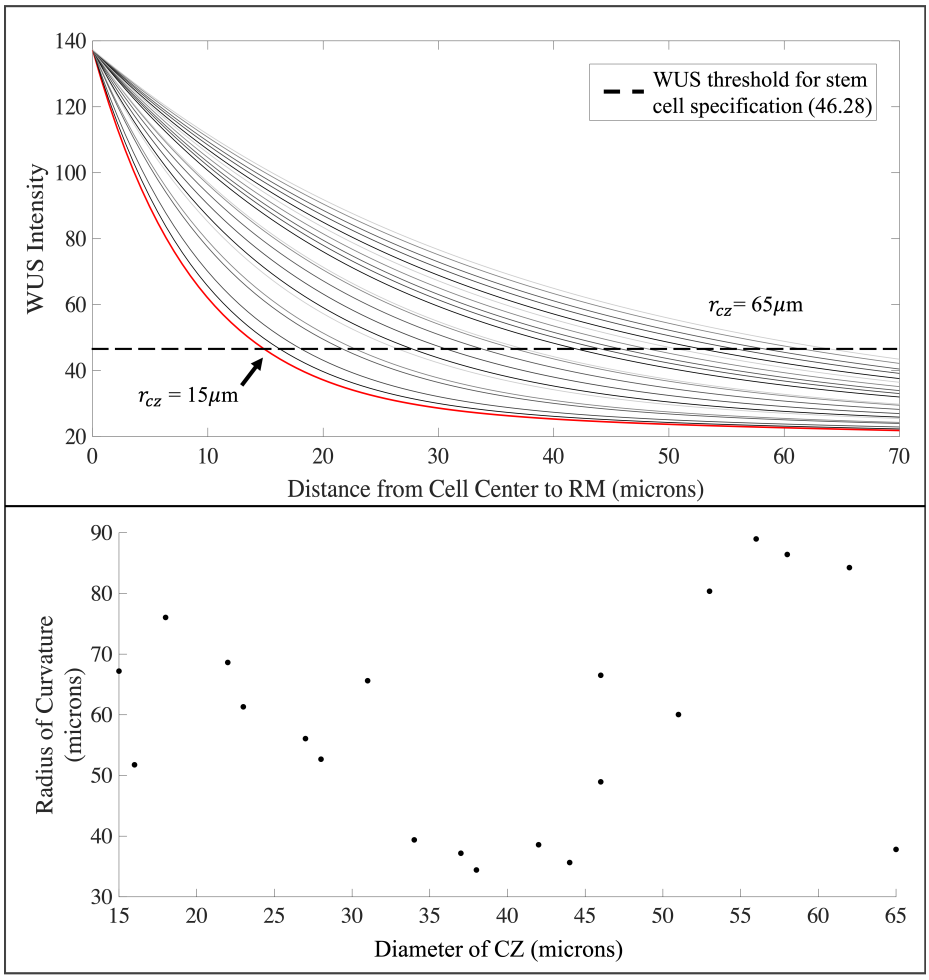

Figure 5.4: Impact of WUS specified stem cell identity on overall tissue shape of SAM. (A) The twenty different functions used as input for the WUS signaling domain in simulations where diameter of CZ is varied. Red line is function used as input for WUS signaling domain in wildtype simulations. Dashed line is WUS threshold for stem cell specification, i.e. cells whose WUS concentration falls above the red line behave as stem cells in simulations. (B) Resulting curvature of the L1 layer of the SAM for each choice of diameter of the CZ from the twenty different simulations. First data point with diameter of the CZ equal to 15μm is average curvature of the L1 layer over five wildtype simulations.

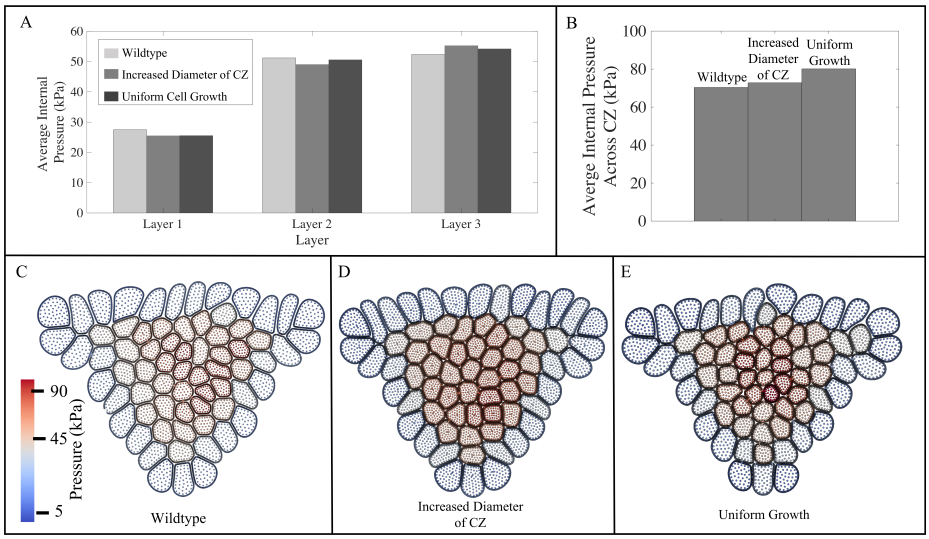

Figure 5.5: Change in pattern of distribution of internal pressure across three different simulations. (A) Distribution of internal pressure across L1, L2 and L3 layers from wildtype, increased diameter of CZ (34 μm $\leq$ diameter $\leq$ 44 μm), and uniform cell growth (diameter of CZ equal to 56μm) simulations. (B) Distribution of internal pressure across CZ from wildtype (avg = 70.32 kPa), increased diameter of CZ (avg = 72.77 kPa), and uniform growth simulations (avg = 80.09 kPa). (C) Distribution of internal pressure in wildtype simulation. (D) Distribution of internal pressure in increased diameter of CZ simulation. (E) Distribution of internal pressure in uniform growth simulation.

tissue could play a role in controlling the rate of cell growth (See section 6.1 for details).

Chapter 6

Conclusions and Future Work

6.1 Biological conclusions from the model simulation results

The growth and development of the SAM depend on spatial and temporal coordination of cell growth patterns, anisotropic cell wall mechanical properties, as well as chemical and mechanical signaling feedbacks controlling cell behavior. In this work, a novel cell-based, SCE model is presented and used for studying morphological implications of individual cell behaviors by analyzing the combined impact of WUS concentration of individual cells controlling cell growth rates and mechanical properties of sub-cellular components of individual cells and the cell wall on the shape of the SAM characterized by the curvature of the L1 layer.

The main novelty of this work is the extension of the general SCE approach to develop a detailed, biologically-calibrated model describing the dynamics of the three layers of the SAM that tests impact of the combined chemical and mechanical effects on regulating SAM growth and shape (See [5] for details). The model combines detailed representations

of cell wall mechanical properties controlling anisotropic cell expansion, deformation of the middle lamella of the cell wall, and increase in cytoplasmic pressure to generate turgor pressure, as well as dynamic interactions between these different sub-cellular components.

In section 5.2.1, model simulations were shown to successfully reproduce emergent properties of the multi-layered SAM tissue including the main axis of expansion of the tissue and average curvature of L1 surface layer of the SAM that matched experiments (Figure 5.2). This provides evidence in support of the hypothesized mechanism of SAM shape formation based on combining layer dependent mechanical anisotropic distribution at the sub-cellular and cellular level with experimentally calibrated diameter of the CZ determining individual cell growth rates as a function of WUS concentration (See [5] for details).

In section 5.2.2, the model was used to successfully test the new hypothesis that WUS concentration of individual cells could impact SAM shape. One of the novel features of the model is the separate representation of individual cells, including cells in the L3 and deeper layers. This makes it possible to test hypotheses about the role of WUS concentration in impacting cell behaviors directly or indirectly by specifying cell identity, especially in the deeper layers where it is difficult to experimentally track cells over time (See [5] for details).

Model predictive simulations demonstrate that significant morphological changes during SAM growth were associated with changes in the diameter of the CZ (Figure 5.4). Moreover, the simulations of WUS concentration-dependent growth could also be linked to its concentration-dependent transcriptional regulation of *CLV3* [89]. This is because earlier analysis revealed that WUS activates *CLV3* transcription at lower concentrations and

represses *CLV3* transcription at higher concentrations [89]. In addition, *CLV3*-mediated signaling is required for nuclear accumulation of WUS in the CZ. Perhaps, *CLV3*-mediated signaling enriching WUS in the nuclei of CZ cells could restrict growth, while the cells in the PZ that are displaced out of the *CLV3*-signaling zone accumulate lower nuclear WUS and divide faster (See [5] for details).

Predictive simulations reveal that meristems with a CZ diameter between 32μm-45μm have a smaller radius of curvature than meristems with a higher CZ diameter ($>$ 45μm) (Figure 5.4)(See [5] for details). These results are consistent with experimental observations wherein ectopic activation of eGFP-WUS in the CZ led to overall lower WUS and an increase in CZ diameter along with an enlarged and pointy meristem (Figure 3.4D and 5.4). Whereas, patches of higher WUS accumulation observed in meristems experiencing ectopic activation of nls-eGFP-WUS led to flatter and irregularly shaped SAMs which could be due to heterogeneity in growth rates and may also be due to the loss of CZ identity in patches (Figure 3.4E and 5.4) [For details see Figure 5C and F in Perales et al. 89]. Though it is unclear whether high WUS concentration of individual cells restricts growth directly or indirectly by specifying cell identity, simulation assumptions that WUS concentration of individual cells controls growth rates are supported by an earlier study from our group showing that direct misexpression of WUS in the PZ leads to retardation of growth [131]. Thus, future time-series data from experiments in combination with additional modeling studies are required to uncouple the impact of cell identity and WUS concentration on growth rates.

In section 5.2.3, predictive model simulations revealed that changes in the size of

the diameter of the CZ resulted in distinct distributions of internal cell pressure across the stem cell niche (Figure 5.5)(See [5] for details). Namely, increasing the diameter of the CZ from 15μm observed in wildtype experiments to 65μm in uniform growth simulations where every cell in the tissue behaves like a stem cell, increased pressure in the CZ by 10 kPa. Model simulation results indicate that cell behavior in response to changes in internal cell pressure could provide an additional mechanism for maintaining the correct ratio of slow growing cells in the CZ to fast growing cells in the PZ resulting in a stable population of stem cells and the correct shape and size of the meristem. More specifically, distribution of pressure in the tissue could play a role in controlling the rate of cell growth and division, i.e. stem cells under higher pressure in the CZ may divide less frequently than differentiated cells under lower pressure in the PZ [124].

To summarize, this work demonstrated using a cell-based model how layer dependent anisotropic mechanical properties of sub-cellular components of individual cells and the cell wall and WUS concentration of individual cells control cell behavior and ultimately determine the final size and shape of the meristem (See [5] for details). Many persisting questions about interactions between chemical and mechanical signaling can be studied using further extensions of the model.

6.2 Future work

6.2.1 Coupled mechanical and dynamic signaling model

In particular, we plan to extend the model by combining the mechanical sub-model with a dynamic signaling model. Understanding how cell growth rates, cell size, cell

shape and cell division patterns facilitate signaling diffusion is crucial for gaining a better understanding of the spatio-temporal regulation of the stem cell niche. For example, the extended model can be used to test the hypothesis that division plane orientation impacts diffusion by the creation of new plasmodesmata in a preferential direction when new cell walls are laid down. If the majority of cells in the deeper L3 layers divide periclinally, the creation of new plasmodesmata along the apical-basal axis of the meristem would create a vertical path for diffusion.

Alternatively, there is evidence that cell wall stiffening may prevent diffusion through plasmodesmata [26]. Performing *in silico* experiments that test the role of plasmodemata-mediated regulation of WUS diffusion in controlling WUS levels could lead to new insights into the plasmodesmata distribution and conductance properties which are otherwise challenging to determine experimentally.

In addition, combining the mechanical sub-model with a dynamic signaling model would make it possible to link sub-cellular processes regulating intracellular WUS distribution to its spatial accumulation and the regulation of *CLV3* transcription. It will also enable us in the future to test the relative roles of WUS, CK and mechanical signals in determining the growth rates and division plane orientation of individual cells. Moreover, new insights as to how cells within a tissue determine the orientation of their plane of division would make it possible to study the effect of division plane orientation on morphological features such as cell growth direction and curvature of the L1 layer of the SAM.

Bibliography

[1] B Alberts, A Johnson, and J Lewis. *Molecular Biology of the Cell*. New York: Garland Science, 2002.

[2] Olivier Ali, Vincent Mirabet, Christophe Godin, and Jan Traas. Physical models of plant development. *Annu. Rev. Cell Dev. Biol.*, 30:59–78, June 2014.

[3] Jun F Allard, J Christian Ambrose, Geoffrey O Wasteneys, and Eric N Cytrynbaum. A mechanochemical model explains interactions between cortical microtubules in plants. *Biophys. J.*, 99(4):1082–1090, August 2010.

[4] Aboutaleb Amiri, Cameron Harvey, Amy Buchmann, Scott Christley, Joshua D Shrout, Igor S Aranson, and Mark Alber. Reversals and collisions optimize protein exchange in bacterial swarms. *Phys Rev E*, 95(3-1):032408, March 2017.

[5] Mikahl Banwarth-Kuhn, Ali Nematbakhsh, Kevin W. Rodriguez, Stephen Snipes, Carolyn G. Rasmussen, G. Venugopala Reddy, and Mark Alber. Cell-based model of the generation and maintenance of the shape and structure of the multilayered shoot apical meristem of arabidopsis thaliana. *Bulletin of Mathematical Biology*, Dec 2018.

[6] M K Barton. Twenty years on: the inner workings of the shoot apical meristem, a developmental dynamo. *Dev. Biol.*, 341(1):95–113, May 2010.

[7] Tobias I Baskin. Anisotropic expansion of the plant cell wall. *Annu. Rev. Cell Dev. Biol.*, 21:203–222, 2005.

[8] K J Bathe and H Saunders. Finite element procedures in engineering analysis, 1984.

[9] Sébastien Besson and Jacques Dumais. Stochasticity in the symmetric division of plant cells: when the exceptions are the rule. *Front. Plant Sci.*, 5:538, October 2014.

[10] N Bessonov and V Volpert. Deformable cell model of tissue growth. *Computation*, 5(4):45, October 2017.

[11] Frédéric Boudon, Jérôme Chopard, Olivier Ali, Benjamin Gilles, Olivier Hamant, Arezki Boudaoud, Jan Traas, and Christophe Godin. A computational framework for 3D mechanical modeling of plant morphogenesis with cellular resolution. *PLoS Comput. Biol.*, 11(1):e1003950, January 2015.

[12] U Brand, J C Fletcher, M Hobe, E M Meyerowitz, and R Simon. Dependence of stem cell fate in arabidopsis on a feedback loop regulated by clv3 activity. *Science*, 289(5479):617–619, 2000.

[13] G W Brodland. How computational models can help unlock biological systems. *Semin. Cell Dev. Biol.*, 47-48:62–73, December 2015.

[14] Amy Buchmann, Mark Alber, and Jeremiah J Zartman. Sizing it up: the mechanical feedback hypothesis of organ growth regulation. *Semin. Cell Dev. Biol.*, 35:73–81, November 2014.

[15] Agata Burian, Michal Ludynia, Magalie Uyttewaal, Jan Traas, Arezki Boudaoud, Olivier Hamant, and Dorota Kwiatkowska. A correlative microscopy approach relates microtubule behaviour, local organ geometry, and cell growth at the arabidopsis shoot apical meristem. *J. Exp. Bot.*, 64(18):5753–5767, December 2013.

[16] Vijay Chickarmane, Adrienne H K Roeder, Paul T Tarr, Alexandre Cunha, Cory Tobin, and Elliot M Meyerowitz. Computational morphodynamics: a modeling framework to understand plant growth. *Annu. Rev. Plant Biol.*, 61:65–87, 2010.

[17] C M Child. EXPERIMENTAL CONTROL OF MORPHOGENESIS IN THE REGULATION OF PLANARIA. *Biol. Bull.*, 20(6):309–331, May 1911.

[18] S Christley, B Lee, X Dai, and Q Nie. Integrative multicellular biological modeling: a case study of 3D epidermal development using GPU algorithms. *BMC Syst. Biol.*, 4:107, August 2010.

[19] Steven E Clark, Robert W Williams, and Elliot M Meyerowitz. The CLAVATA1Gene encodes a putative receptor kinase that controls shoot and floral meristem size in arabidopsis. *Cell*, 89(4):575–585, May 1997.

[20] Enrico Coen, Anne-Gaëlle Rolland-Lagan, Mark Matthews, J Andrew Bangham, and Przemyslaw Prusinkiewicz. The genetics of geometry. *Proc. Natl. Acad. Sci. U. S. A.*, 101(14):4728–4735, April 2004.

[21] Francis Corson, Mokhtar Adda-Bedia, and Arezki Boudaoud. In silico leaf venation networks: growth and reorganization driven by mechanical forces. *J. Theor. Biol.*, 259(3):440–448, August 2009.

[22] Francis Corson, Olivier Hamant, Steffen Bohn, Jan Traas, Arezki Boudaoud, and Yves Couder. Turning a plant tissue into a living cell froth through isotropic growth. *Proc. Natl. Acad. Sci. U. S. A.*, 106(21):8453–8458, May 2009.

[23] D J Cosgrove. Wall structure and wall loosening. a look backwards and forwards. *Plant Physiol.*, 125(1):131–134, January 2001.

[24] Daniel J Cosgrove. Growth of the plant cell wall. *Nat. Rev. Mol. Cell Biol.*, 6(11):850–861, November 2005.

[25] F B Daher and S A Braybrook. How to let go: pectin and plant cell adhesion. *Frontiers in plant science*, 6:523, 2015.

[26] Gabor Daum, Anna Medzihradszky, Takuya Suzaki, and Jan U Lohmann. A mechanistic framework for noncell autonomous stem cell induction in arabidopsis. *Proc. Natl. Acad. Sci. U. S. A.*, 111(40):14619–14624, October 2014.

[27] P B de Reuille, I Bohn-Courseau, K Ljung, H Morin, N Carraro, C Godin, and J Traas. Computer simulations reveal properties of the cell-cell signaling network at the shoot apex in arabidopsis. *Proceedings of the National Academy of Sciences*, 103(5):1627–1632, 2006.

[28] M C Diaz de la Loza and B J Thompson. Forces shaping the drosophila wing. *Mech. Dev.*, 144(Pt A):23–32, April 2017.

[29] Jacques Dumais, Sidney L Shaw, Charles R Steele, Sharon R Long, and Peter M Ray. An anisotropic-viscoplastic model of plant cell morphogenesis by tip growth. *Int. J. Dev. Biol.*, 50(2-3):209–222, 2006.

[30] Lionel Dupuy, Jonathan Mackenzie, and Jim Haseloff. Coordination of plant cell division and expansion in a simple morphogenetic system. *Proc. Natl. Acad. Sci. U. S. A.*, 107(6):2711–2716, February 2010.

[31] Lionel Dupuy, Jonathan Mackenzie, Tim Rudge, and Jim Haseloff. A system for modelling Cell–Cell interactions during plant morphogenesis. *Ann. Bot.*, 101(8):1255–1265, May 2008.

[32] Lionel Dupuy, Jonathan P Mackenzie, and Jim P Haseloff. A biomechanical model for the study of plant morphogenesis: Coleocheate orbicularis, a 2D study species. In *Proceedings of the 5th Plant Biomechanics Conference, Stockholm, Sweden*, 2006.

[33] R J Dyson and O E Jensen. A fibre-reinforced fluid model of anisotropic plant cell growth. *J. Fluid Mech.*, 655:472–503, July 2010.

[34] Ralph O Erickson. Modeling of plant growth. *Annu. Rev. Plant Physiol.*, 27(1):407–434, 1976.

[35] L Errera. Uber zellformen und seifenblasen. *Bot. Centralbl.*, 34:395–398, 1888.

[36] Reza Farhadifar, Jens-Christian Röper, Benoit Aigouy, Suzanne Eaton, and Frank Jülicher. The influence of cell mechanics, cell-cell interactions, and proliferation on epithelial packing. *Curr. Biol.*, 17(24):2095–2104, December 2007.

[37] K N Farrell. Steering into the skid: the challenge of operationalising type II error avoidance in science for policy. *Paper in progress*, 2007.

[38] A G Fletcher, F Cooper, and R E Baker. Mechanocellular models of epithelial morphogenesis. *Philos. Trans. R. Soc. Lond. B Biol. Sci.*, 372(1720), May 2017.

[39] J C Fletcher, U Brand, M P Running, R Simon, and E M Meyerowitz. Signaling of cell fate decisions by CLAVATA3 in arabidopsis shoot meristems. *Science*, 283(5409):1911–1914, March 1999.

[40] John A Fozard, Mikaël Lucas, John R King, and Oliver E Jensen. Vertex-element models for anisotropic growth of elongated plant organs. *Front. Plant Sci.*, 4:233, July 2013.

[41] Anja Geitmann. Experimental approaches used to quantify physical parameters at cellular and subcellular levels. *Am. J. Bot.*, 93(10):1380–1390, October 2006.

[42] A Gierer and H Meinhardt. A theory of biological pattern formation. *Kybernetik*, 12(1):30–39, December 1972.

[43] A Gord, W R Holmes, X Dai, and Q Nie. Computational modelling of epidermal stratification highlights the importance of asymmetric cell division for predictable and robust layer formation. *Journal of the Royal Society Interface*, 11(99):20140631, 2014.

[44] Adrien Guérin, Simon Gravelle, and Jacques Dumais. Forces behind plant cell division. *Proc. Natl. Acad. Sci. U. S. A.*, 113(32):8891–8893, August 2016.

[45] Olivier Hamant, Marcus G Heisler, Henrik Jönsson, Pawel Krupinski, Magalie Uyttewaal, Plamen Bokov, Francis Corson, Patrik Sahlin, Arezki Boudaoud, Elliot M Meyerowitz, Yves Couder, and Jan Traas. Developmental patterning by mechanical signals in arabidopsis. *Science*, 322(5908):1650–1655, December 2008.

[46] Olivier Hamant and Jan Traas. The mechanics behind plant development. *New Phytol.*, 185(2):369–385, January 2010.

[47] Davide Heller, Andreas Hoppe, Simon Restrepo, Lorenzo Gatti, Alexander L Tournier, Nicolas Tapon, Konrad Basler, and Yanlan Mao. EpiTools: An Open-Source image analysis toolkit for quantifying epithelial growth dynamics. *Dev. Cell*, 36(1):103–116, January 2016.

[48] Jukka Jernvall and Others. A gene network model accounting for development and evolution of mammalian teeth. *Proceedings of the National Academy of Sciences*, 99(12):8116–8120, 2002.

[49] Ting-Xin Jiang, Randall B Widelitz, Wei-Min Shen, Peter Will, Da-Yu Wu, Chih-Min Lin, Han-Sung Jung, and Cheng-Ming Chuong. Integument pattern formation involves genetic and epigenetic controls: feather arrays simulated by digital hormone models. *Int. J. Dev. Biol.*, 48(2-3):117–135, 2004.

[50] H Jönsson, M Heisler, G V Reddy, V Agrawal, V Gor, B E Shapiro, E Mjolsness, and E M Meyerowitz. Modeling the organization of the wuschel expression domain in the shoot apical meristem. *Bioinformatics*, 21(suppl_1):i232–i240, 2005.

[51] Henrik Jönsson, Jérémy Gruel, Pawel Krupinski, and Carl Troein. On evaluating models in computational morphodynamics. *Curr. Opin. Plant Biol.*, 15(1):103–110, February 2012.

[52] Henrik Jönsson, Marcus G Heisler, Bruce E Shapiro, Elliot M Meyerowitz, and Eric Mjolsness. An auxin-driven polarized transport model for phyllotaxis. *Proc. Natl. Acad. Sci. U. S. A.*, 103(5):1633–1638, January 2006.

[53] E F Keller and L A Segel. Model for chemotaxis. *J. Theor. Biol.*, 30(2):225–234, February 1971.

[54] Richard Kennaway, Enrico Coen, Amelia Green, and Andrew Bangham. Generation of diverse biological forms through combinatorial interactions between tissue polarity and growth. *PLoS Comput. Biol.*, 7(6):e1002071, June 2011.

[55] Shigeru Kondo and Takashi Miura. Reaction-diffusion model as a framework for understanding biological pattern formation. *Science*, 329(5999):1616–1620, September 2010.

[56] Robert W Korn and Richard M Spalding. THE GEOMETRY OF PLANT EPIDERMAL CELLS. *New Phytol.*, 72(6):1357–1365, November 1973.

[57] Jochen Kursawe, Pavel A Brodskiy, Jeremiah J Zartman, Ruth E Baker, and Alexander G Fletcher. Capabilities and limitations of tissue size control through passive mechanical forces. *PLoS Comput. Biol.*, 11(12):e1004679, December 2015.

[58] T Laux, K F Mayer, J Berger, and G Jürgens. The WUSCHEL gene is required for shoot and floral meristem integrity in arabidopsis. *Development*, 122(1):87–96, January 1996.

[59] Z Liu, S Persson, and C Sánchez-Rodríguez. At the border: the plasma membrane–cell wall continuum. *Journal of experimental botany*, 66(6):1553–1563, 2015.

[60] J A Lockhart. An analysis of irreversible plant cell elongation. *J. Theor. Biol.*, 8(2):264–275, March 1965.

[61] M Louveaux and O Hamant. The mechanics behind cell division. *Curr. Opin. Plant Biol.*, 16(6):774–779, December 2013.

[62] M Louveaux, J D Julien, V Mirabet, A Boudaoud, and O Hamant. Cell division plane orientation based on tensile stress in arabidopsis thaliana. *Proceedings of the National Academy of Sciences*, 113(30):E4294–E4303, 2016.

[63] Robert F Lyndon and Others. *The shoot apical meristem: its growth and development*. Cambridge University Press, 1998.

[64] Philip K Maini, Kevin J Painter, and Helene Nguyen Phong Chau. Spatial pattern formation in chemical and biological systems. *J. Chem. Soc. Faraday Trans.*,

93(20):3601–3610, 1997.

[65] Simeone Marino, Ian B Hogue, Christian J Ray, and Denise E Kirschner. A methodology for performing global uncertainty and sensitivity analysis in systems biology. *J. Theor. Biol.*, 254(1):178–196, September 2008.

[66] MATLAB. *version 9.4 (R2018b)*. The MathWorks Inc., Natick, Massachusetts, 2018.

[67] K F Mayer, H Schoof, A Haecker, M Lenhard, G Jürgens, and T Laux. Role of WUSCHEL in regulating stem cell fate in the arabidopsis shoot meristem. *Cell*, 95(6):805–815, December 1998.

[68] M D McKay, R J Beckman, and W J Conover. A comparison of three methods for selecting values of input variables in the analysis of output from a computer code, 1979.

[69] H Meinhardt. Models of biological pattern formation. 1982.

[70] Hans Meinhardt. *The Algorithmic Beauty of Sea Shells*. Springer Science & Business Media, August 2009.

[71] Roeland M H Merks, Michael Guravage, Dirk Inzé, and Gerrit T S Beemster. VirtualLeaf: an open-source framework for cell-based modeling of plant tissue growth and development. *Plant Physiol.*, 155(2):656–666, February 2011.

[72] E M Meyerowitz. Plants, animals and the logic of development. *Trends Cell Biol.*, 9(12):M65–8, December 1999.

[73] F Milde, G Tauriello, H Haberkern, and P Koumoutsakos. SEM++: A particle model of cellular growth, signaling and migration. *Computational Particle Mechanics*, 1(2):211–227, June 2014.

[74] A R Mitchell. Finite elements: An introduction. volume 1, e. b. becker, g. f. carey and j. t. oden, Prentice-Hall. *Int. J. Numer. Meth. Engng.*, 18(6):954–955, June 1982.

[75] Eric Mjolsness and Guy Yosiphon. Stochastic process semantics for dynamical grammars. *Ann. Math. Artif. Intell.*, 47(3-4):329–395, August 2006.

[76] P M Morse. Diatomic molecules according to the wave mechanics. ii. vibrational levels. *Physical Review*, 34(1):57, 1929.

[77] R Müller, L Borghi, D Kwiatkowska, P Laufs, and R Simon. Dynamic and compensatory responses of arabidopsis shoot and floral meristems to clv3 signaling. *The Plant Cell*, 18(5):1188–1198, 2006.

[78] Ali Nematbakhsh, Wenzhao Sun, Pavel A Brodskiy, Aboutaleb Amiri, Cody Narciso, Zhiliang Xu, Jeremiah J Zartman, and Mark Alber. Multi-scale computational study of the mechanical regulation of cell mitotic rounding in epithelia. *PLoS Comput. Biol.*,

13(5):e1005533, May 2017.

[79] T Newman. Modeling multicellular structures using the subcellular element model. In *Single-Cell-Based Models in Biology and Medicine*, pages 221–239. Springer, 2007.

[80] T J Newman. Modeling multicellular systems using subcellular elements. *Math. Biosci. Eng.*, 2(3):613–624, July 2005.

[81] H F Nijhout. The control of growth, 2003.

[82] K J Niklas. Applications of finite element analyses to problems in plant morphology. *Ann. Bot.*, 1977.

[83] Mari Ogawa, Hidefumi Shinohara, Youji Sakagami, and Yoshikatsu Matsubayashi. Arabidopsis CLV3 peptide directly binds CLV1 ectodomain. *Science*, 319(5861):294, January 2008.

[84] S Oldham, R Böhni, H Stocker, W Brogiolo, and E Hafen. Genetic control of size in drosophila. *Philos. Trans. R. Soc. Lond. B Biol. Sci.*, 355(1399):945–952, July 2000.

[85] Sophie Pantalacci, Marie Sémon, Arnaud Martin, Pascale Chevret, and Vincent Laudet. Heterochronic shifts explain variations in a sequentially developing repeated pattern: palatal ridges of muroid rodents. *Evol. Dev.*, 11(4):422–433, July 2009.

[86] Alexander R Paredez, Christopher R Somerville, and David W Ehrhardt. Visualization of cellulose synthase demonstrates functional association with microtubules. *Science*, 312(5779):1491–1495, June 2006.

[87] Joseph Parker. Morphogens, nutrients, and the basis of organ scaling. *Evol. Dev.*, 13(3):304–314, May 2011.

[88] P Pathmanathan, J Cooper, A Fletcher, G Mirams, P Murray, J Osborne, J Pitt-Francis, A Walter, and S J Chapman. A computational study of discrete mechanical tissue models. *Physical biology*, 6(3):036001, 2009.

[89] M Perales, K Rodriguez, S Snipes, R K Yadav, M Diaz-Mendoza, and G V Reddy. Threshold-dependent transcriptional discrimination underlies stem cell homeostasis. *Proceedings of the National Academy of Sciences*, 113(41):E6298–E6306, 2016.

[90] Przemyslaw Prusinkiewicz and Adam Runions. Computational models of plant development and form. *New Phytol.*, 193(3):549–569, February 2012.

[91] C G Rasmussen, A J Wright, and S Müller. The role of the cytoskeleton and associated proteins in determination of the plant cell division plane. *Plant J.*, 75(2):258–269, July 2013.

[92] G Venugopala Reddy, Marcus G Heisler, David W Ehrhardt, and Elliot M Meyerowitz. Real-time lineage analysis reveals oriented cell divisions associated with morphogen-

esis at the shoot apex of arabidopsis thaliana. *Development*, 131(17):4225–4237, September 2004.

[93] G Venugopala Reddy and Elliot M Meyerowitz. Stem-cell homeostasis and growth dynamics can be uncoupled in the arabidopsis shoot apex. *Science*, 310(5748):663–667, October 2005.

[94] D Reinhardt, E R Pesce, P Stieger, T Mandel, K Baltensperger, M Bennett, J Traas, J Friml, and C Kuhlemeier. Regulation of phyllotaxis by polar auxin transport. *Nature*, 426(6964):255, 2003.

[95] K Rodriguez, M Perales, S Snipes, R K Yadav, M Diaz-Mendoza, and G V Reddy. Dna-dependent homodimerization, sub-cellular partitioning, and protein destabilization control wuschel levels and spatial patterning. *Proceedings of the National Academy of Sciences*, 113(41):E6307–E6315, 2016.

[96] Katherine W Rogers and Alexander F Schier. Morphogen gradients: from generation to interpretation. *Annu. Rev. Cell Dev. Biol.*, 27:377–407, July 2011.

[97] Anne-Lise Routier-Kierzkowska and Richard S Smith. Measuring the mechanics of morphogenesis. *Curr. Opin. Plant Biol.*, 16(1):25–32, February 2013.

[98] Julius Sachs. Uber die anordnung der zellen in jungsten pflanzentheilen. *Arb. Bot. Inst. Wurzburg*, 2:46–104, 1878.

[99] T Sachs. Polarity changes and tissue organization in plants. In *International Cell Biology 1980–1981*, pages 489–496. Springer Berlin Heidelberg, 1981.

[100] Andrea Saltelli, Marco Ratto, Terry Andres, Francesca Campolongo, Jessica Cariboni, Debora Gatelli, Michaela Saisana, and Stefano Tarantola. *Global sensitivity analysis: the primer*. John Wiley & Sons, 2008.

[101] A Sampathkumar, P Krupinski, R Wightman, P Milani, A Berquand, A Boudaoud, O Hamant, H Jönsson, and E M Meyerowitz. Subcellular and supracellular mechanical stress prescribes cytoskeleton behavior in arabidopsis cotyledon pavement cells. *Elife*, 3:e01967, April 2014.

[102] Arun Sampathkumar, Pawel Krupinski, Raymond Wightman, Pascale Milani, Alexandre Berquand, Arezki Boudaoud, Olivier Hamant, Henrik Jönsson, and Elliot M Meyerowitz. Subcellular and supracellular mechanical stress prescribes cytoskeleton behavior in arabidopsis cotyledon pavement cells. *Elife*, 3:e01967, April 2014.

[103] Arun Sampathkumar, An Yan, Pawel Krupinski, and Elliot M Meyerowitz. Physical forces regulate plant development and morphogenesis. *Curr. Biol.*, 24(10):R475–83, May 2014.

[104] S Sandersius, M Chuai, C J Weijer, and T Newman. Correlating cell behavior with tissue topology in embryonic epithelia. *PLoS One*, 6(4):e18081, April 2011.

[105] S Sandersius and T Newman. Modeling cell rheology with the subcellular element model. *Physical biology*, 5(1):015002, 2008.

[106] S Sandersius, C Weijer, and T Newman. Emergent cell and tissue dynamics from subcellular modeling of active biomechanical processes. *Phys. Biol.*, 8(4):045007, August 2011.

[107] Schiff. *Quantum mechanics*. McGraw-Hill Education (India) Pvt Limited, 1968.

[108] Gerald Schwank and Konrad Basler. Regulation of organ growth by morphogen gradients. *Cold Spring Harb. Perspect. Biol.*, 2(1):a001669, January 2010.

[109] Laura Serna and Carmen Fenoll. Stomatal precursors in arabidopsis: prohibiting the fulfilment of a general rule: Letters. *New Phytol.*, 158(3):427–430, May 2003.

[110] Stefanie Sick, Stefan Reinker, Jens Timmer, and Thomas Schlake. WNT and DKK determine hair follicle spacing through a reaction-diffusion mechanism. *Science*, 314(5804):1447–1450, December 2006.

[111] L G Smith. Cell division: Plant cell division: building walls in the right places. *Nature Reviews Molecular Cell Biology*, 2(1):33, 2001.

[112] R S Smith, S Guyomarc'h, Th Mandel, D Reinhardt, C Kuhlemeier, and P Prusinkiewicz. A plausible model of phyllotaxis. *Proceedings of the National Academy of Sciences*, 103(5):1301–1306, 2006.

[113] Stephen A Snipes, Kevin Rodriguez, Aaron E DeVries, Kaori N Miyawaki, Mariano Perales, Mingtang Xie, and G Venugopala Reddy. Cytokinin stabilizes WUSCHEL by acting on the protein domains required for nuclear enrichment and transcription. *PLoS Genet.*, 14(4):e1007351, April 2018.

[114] B Z Stanger. The biology of organ size determination. *Diabetes Obes. Metab.*, 10 Suppl 4:16–22, November 2008.

[115] Taylor A Steeves and Ian M Sussex. *Patterns in Plant Development*. Cambridge University Press, July 1989.

[116] Christopher R Sweet, Santanu Chatterjee, Zhiliang Xu, Katharine Bisordi, Elliot D Rosen, and Mark Alber. Modelling platelet-blood flow interaction using the subcellular element langevin method. *J. R. Soc. Interface*, 8(65):1760–1771, December 2011.

[117] S Tanaka. Simulation frameworks for morphogenetic problems. *Computation*, 3(2):197–221, April 2015.

[118] D'Arcy Wentworth Thompson. *On growth and form / by D'Arcy Wentworth Thompson*. Cambridge University Press Cambridge, Eng, 2nd ed. edition, 1942.

[119] J Truskina and T Vernoux. The growth of a stable stationary structure: coordinating cell behavior and patterning at the shoot apical meristem. *Current opinion in plant biology*, 41:83–88, 2018.

[120] A M Turing. The chemical basis of morphogenesis. 1953. *Bull. Math. Biol.*, 52(1-2):153–97; discussion 119–52, 1990.

[121] M Uyttewaal, K Burian, Aand Alim, B Landrein, D Borowska-Wykret, A Dedieu, A Peaucelle, M Ludynia, J Traas, and A Boudaoud. Mechanical stress acts via katanin to amplify differences in growth rate between adjacent cells in arabidopsis. *Cell*, 149(2):439–451, 2012.

[122] P Van Liedekerke, M M Palm, N Jagiella, and D Drasdo. Simulating tissue mechanics with agent-based models: concepts, perspectives and some novel results. *Computational Particle Mechanics*, 2(4):401–444, 2015.

[123] F Vermolen and A Gefen. A semi-stochastic cell-based formalism to model the dynamics of migration of cells in colonies. *Biomech. Model. Mechanobiol.*, 11(1-2):183–195, January 2012.

[124] J Vollmer, F Casares, and D. Iber. Growth and size control during development. *Open Biol.*, 7(11), November 2017.

[125] R E Williamson. Alignment of cortical microtubules by anisotropic wall stresses. *Funct. Plant Biol.*, 17(6):601–613, 1990.

[126] L Wolpert. Positional information and the spatial pattern of cellular differentiation. *J. Theor. Biol.*, 25(1):1–47, October 1969.

[127] F Wottawah, S Schinkinger, B Lincoln, R Ananthakrishnan, M Romeyke, J Guck, and J Käs. Optical rheology of biological cells. *Physical review letters*, 94(9):098103, 2005.

[128] Ziheng Wu, Zhiliang Xu, Oleg Kim, and Mark Alber. Three-dimensional multi-scale model of deformable platelets adhesion to vessel wall in blood flow. *Philos. Trans. A Math. Phys. Eng. Sci.*, 372(2021), August 2014.

[129] Mingtang Xie, Moses Tataw, and G Venugopala Reddy. Towards a functional understanding of cell growth dynamics in shoot meristem stem-cell niche. *Semin. Cell Dev. Biol.*, 20(9):1126–1133, December 2009.

[130] Ram Kishor Yadav, Mariano Perales, Jérémy Gruel, Thomas Girke, Henrik Jönsson, and G Venugopala Reddy. WUSCHEL protein movement mediates stem cell homeostasis in the arabidopsis shoot apex. *Genes Dev.*, 25(19):2025–2030, October 2011.

[131] Ram Kishor Yadav, Montreh Tavakkoli, and G Venugopala Reddy. WUSCHEL mediates stem cell homeostasis by regulating stem cell number and patterns of cell division and differentiation of stem cell progenitors. *Development*, 137(21):3581–3589, Novem-

ber 2010.

[132] Ram Kishor Yadav, Montreh Tavakkoli, Mingtang Xie, Thomas Girke, and G Venugopala Reddy. A high-resolution gene expression map of the arabidopsis shoot meristem stem cell niche. *Development*, 141(13):2735–2744, July 2014.

[133] Motoomi Yamaguchi, Eiichi Yoshimoto, and Shigeru Kondo. Pattern regulation in the stripe of zebrafish suggests an underlying dynamic and autonomous mechanism. *Proc. Natl. Acad. Sci. U. S. A.*, 104(12):4790–4793, March 2007.

[134] Yong-Tao Zhang, Mark S Alber, and Stuart A Newman. Mathematical modeling of vertebrate limb development. *Math. Biosci.*, 243(1):1–17, May 2013.

[135] Jianfeng Zhu, Yong-Tao Zhang, Mark S Alber, and Stuart A Newman. Bare bones pattern formation: a core regulatory network in varying geometries reproduces major features of vertebrate limb development and evolution. *PLoS One*, 5(5):e10892, May 2010.

Appendix A

Flowchart Outlining the Computational Implementation of the Model

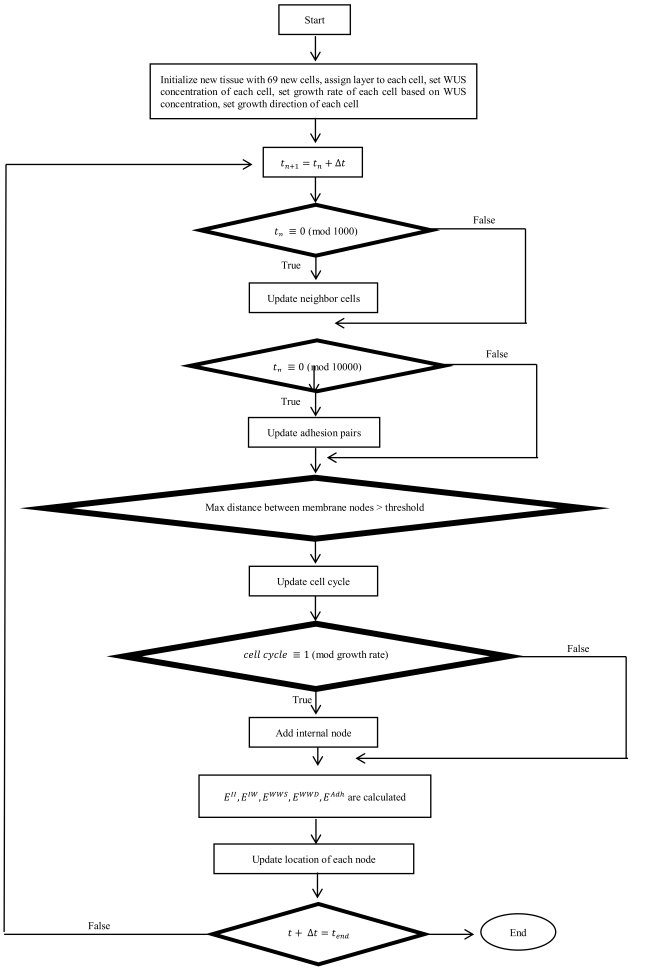

Fig A1.1 Flowchart of the model implemented in C++.